Journal of Medicinal Chemistry

pubs.acs.org/jmc

Article

High-Affinity and Proteolytically Stable Peptidic Fluorescent NTS_1R Ligands

Fabian J. Ertl, Anna Friedel, Elena J. Schmid, Carina Höring, Nataliya Archipowa, Pierre Koch, Simone Maschauer, Roger J. Kutta,* Olaf Prante,* and Max Keller*

Cite This: https://doi.org/10.1021/acs.jmedchem.5c01701

Read Online

ACCESS | Metrics & More | Article Recommendations | Supporting Information

ABSTRACT: Labeled ligands for the neurotensin receptor 1 (NTS_1R), which is expressed in the CNS, the gastrointestinal tract, and in malignant tumors, are needed to investigate NTS_1R-ligand binding and NTS_1R expression. Aiming for fluorescence-labeled neurotensin(8−13)-derived NTS_1R ligands with high affinity and proteolytic stability, several previous approaches were combined: (1) replacement of Arg^8 by an amino-functionalized carbamoylated arginine, allowing conjugation to a fluorophore, (2) N^{α}-methylation of Arg^8 and replacement of Tyr by β,β-dimethyl-L-Tyr^{11}, conferring proteolytic stability, and (3) replacement of Leu^{13} by trimethylsilyl-Ala, boosting binding affinity. This strategy gave fluorescent NTS_1R ligands with unprecedented NTS_1R binding affinity (5-TAMRA-labeled ligand **19**: K_i 0.14 nM, sulfo-Cy5-labeled probe **21**: K_i 0.094 nM) and high stability in human plasma ($t_{1/2} \gg 48$ h). Their suitability for competition binding studies (flow cytometry; **19**, **21**) and the imaging of NTS_1R expression in living cells (confocal microscopy, biomolecular imaging; **19**, **21**) and tumor tissue (biomolecular imaging; **21**) is demonstrated.

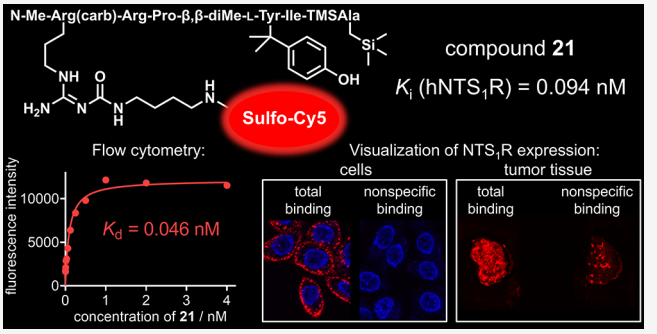

INTRODUCTION

The neurotensin receptor 1 (NTS_1R), a class A G-protein coupled receptor (GPCR), is one of three receptors of the neurotensin receptor family. The hexapeptide neuromedin N and the tridecapeptide neurotensin (NT) represent endogenous NTS_1R agonists (Figure 1A). The bioactivity of neurotensin is conferred by the C-terminal hexapeptide sequence, NT(8−13).[1] Thus, NT(8−13) has served as a lead structure for the development of various NTS_1R ligands including radio- and fluorescence labeled analogs. In healthy tissues, the NTS_1R is mainly expressed in the brain and gastrointestinal tract.[2,3] With regard to neoplastic diseases, the NTS_1R is (over)expressed, e.g., in pancreatic adenocarcinoma, prostate and colon carcinoma, and in about one-third of primary breast cancer tumors.[4−9] Therefore, the NTS_1R is considered a promising target for tumor diagnostics and treatment using metabolically stable, appropriately radiolabeled NTS_1R ligands.[10]

Besides radioligands, fluorescently labeled NTS_1R ligands also represent useful tool compounds which can substitute radioligands, e.g., in competition binding assays needed to determine binding affinities of new NTS_1R ligands. Advantages of fluorescent probes over radioligands are mild safety issues, unproblematic waste disposal, and accessibility to a broad range of methods such as flow cytometry, high-content imaging, fluorescence anisotropy or NanoBRET, most of them being compatible with multimode plate reader measurements. Moreover, fluorescent probes can be used to study receptor−ligand binding by fluorescence microscopy. Unlike radiochemical assays, most fluorescence-based techniques allow for measurement under homogeneous conditions, meaning that a separation of bound from free ligand is not required.

To date, several fluorescent NTS_1R ligands, all derived from NT(8−13), have been reported (e.g., **1**−**4**, Figure 1B). These probes were characterized by high-content imaging, flow cytometry, fluorescence anisotropy, NanoBRET or fluorescence microscopy.[11−16] Among the reported fluorescently labeled NTS_1R ligands, compounds **1**−**3** exhibit the highest binding affinities (K_i = 0.76−1.1 nM) allowing an application as probes for cell-based binding assays.

Yet, there is interest in fluorescently labeled NTS_1R ligands with even higher binding affinity since this comes along with reduced nonspecific binding and potentially with longer residence time, which is particularly advantageous for fluorescence-based imaging of receptor expression, e.g., in tumor tissue.

Received: June 20, 2025
Revised: August 5, 2025
Accepted: August 18, 2025

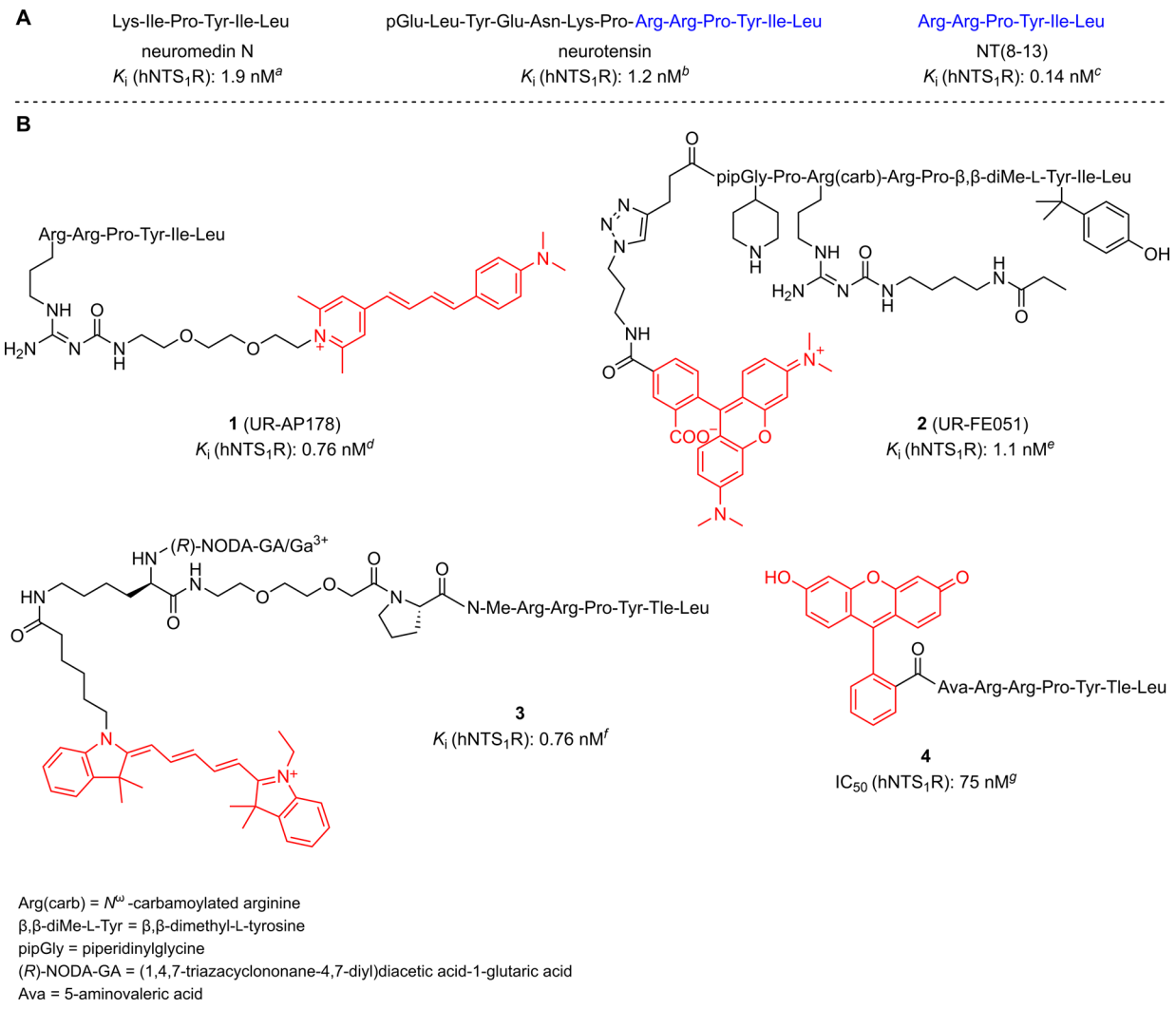

Figure 1. (A) Peptide sequences and NTS_1R binding affinities of the endogenous NTS_1R ligands neuromedin N and neurotensin, and the lead compound NT(8−13). (B) Reported fluorescent NTS_1R ligands with binding affinities in the low nanomolar range. Fluorescent dyes are shown in red. [a]Skrzydelski et al.,[17] [b]Granier et al.,[18] [c]Keller et al.,[12] [d]Keller et al.,[13] [e]Ertl et al.,[16] [f]Renard et al.,[14] [g]Maes et al.[11]

The design of the novel fluorescently labeled NT(8−13)-derivatives in this study was guided by different reported studies. First, Leu[13] is replaced by (trimethylsilyl)alanine (TMSAla) in the synthesized NT(8−13) analogs because Fanelli and coworkers reported that this structural modification leads to markedly increased NTS_1R binding affinity of hexapeptides derived from NT(8−13) (see compounds **5** and **6**, Figure 2).[19]

Second, Arg[8] is bioisosterically exchanged by an amino-functionalized N^{ω}-carbamoylated arginine (Arg(carb)) (e.g., compound **7**, Figure 2).[12] Attachment of fluorescent dyes to the side chain of this carbamoylated arginine was previously demonstrated to be well tolerated with respect to NTS_1R binding.[13,16] Third, the N-terminus is methylated and Tyr[11] is replaced by *β,β*-dimethyltyrosine, in order to obtain proteolytically stable peptides. The N-terminal methylation was reported to prevent N-terminal degradation by proteases[22] and the incorporation of *β,β*-dimethyl-Tyr was recently shown to result in an effective stabilization of the C-terminus against proteolytic cleavage (see compounds **8** and **9**, Figure 2).[21] Notably, the replacement of Tyr[11] by *β,β*-dimethyl-Tyr represents a favorable alternative to the replacement of Ile[12] by *α-tert*-butylglycine (standard modification for the stabilization of the C-terminus), since NTS_1R binding is affected by the latter but not by the former modification.[21]

For fluorescence labeling of the peptides, the rhodamine-based dye 5-TAMRA and the indolinium-type cyanine dye sulfo-Cy5 were used. The precursor compounds and the labeled peptides were characterized in a radiochemical NTS_1R competition binding assay. The labeled probes were also studied in a functional NTS_1R Ca^{2+} assay and were photophysically characterized (fluorescent quantum yields and fluorescence lifetimes). Moreover, NTS_1R binding of the fluorescent ligands was investigated by flow cytometry (saturation binding, kinetic studies, and competition binding), confocal microscopy, and in tumor sections using a biomolecular imager.

RESULTS AND DISCUSSION

Synthesis. The unnatural, Fmoc-protected amino acids (**10**−**13**) used for the peptide synthesis are shown in Scheme 1A. N^{α}-methylated Fmoc/Pbf-protected arginine (**11**) and racemic Fmoc/*t*Bu-protected *β,β*-dimethyl-Tyr (**12**) were commercially available (note: the desired L-configured stereoisomer of **12** was not available as a pure enantiomer). The Fmoc/Boc-protected amino-functionalized, carbamoylated

https://doi.org/10.1021/acs.jmedchem.5c01701
J. Med. Chem. XXXX, XXX, XXX−XXX

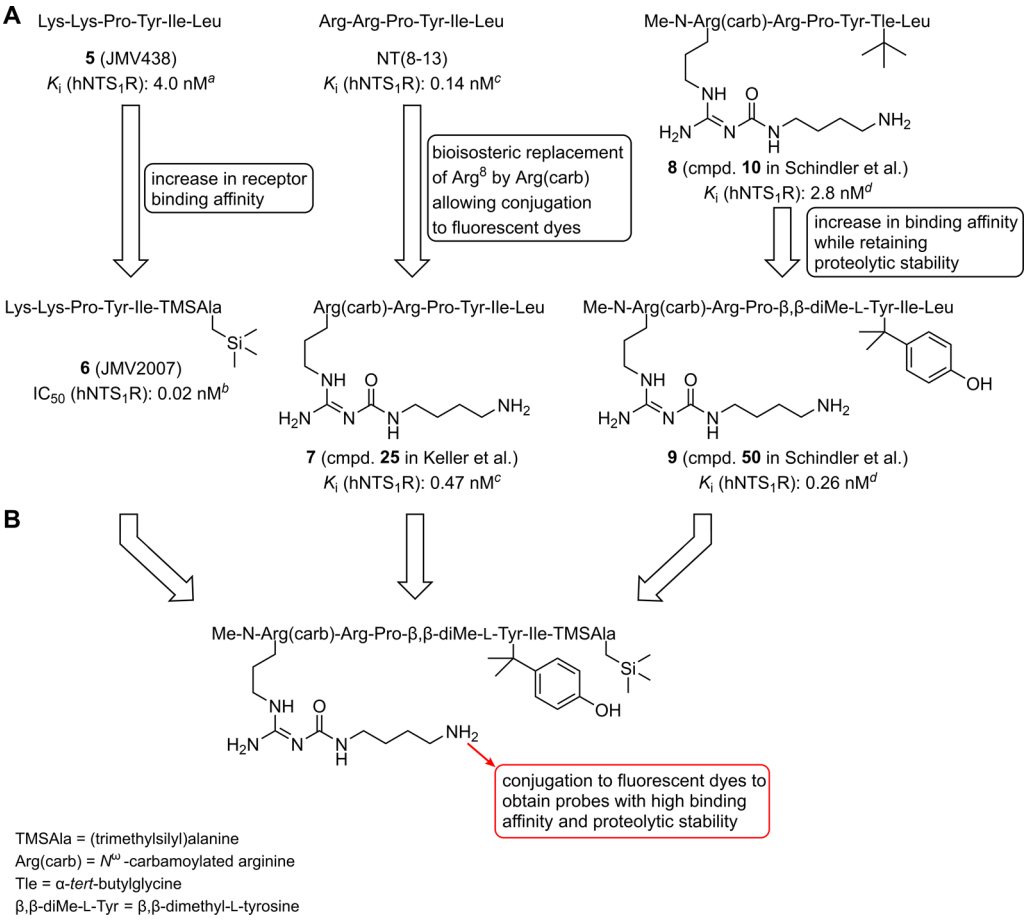

Figure 2. (A) Schematic presentation of reported amino acid replacements in NT(8−13) or NT(8−13) derivatives useful to increase NTS_1R binding affinity (replacement of Leu[13] by TMSAla), for peptide conjugation (replacement of Arg[8] by an amino-functionalized carbamoylated arginine), and to achieve proteolytic stability (methylation of the N-terminus and replacement of Tyr[11] by *β,β*-dimethyl-L-Tyr). (B) Aim of the present study: combination of approaches shown in A in one molecule followed by the synthesis of fluorescently labeled NTS_1R ligands. [a]Vivancos et al.,[20] [b]Fanelli et al.,[19] [c]Keller et al.,[12] [d]Schindler et al.[21]

arginine (**13**) was prepared as reported.[12] The Fmoc-protected TMSAla (**10**) was synthesized according to a published procedure yielding (*R*)-**10** with a reported ee of 98%.[23] Here, this asymmetric synthesis, using (1*R*,2*R*,5*R*)-2-hydroxy-3-pinanone (**23**) as chiral auxiliary (see Scheme S1), gave (*R*)-**10** with an ee of 86% (determined with capillary electrophoresis, electropherograms shown in the Supporting Information).

All peptides (**6**, **14**−**17b**; sequences shown in Scheme 1B) were synthesized by solid-phase peptide synthesis (SPPS) on a 2-ClTrt resin. Peptide **14** represents the NT(8−13) derivative containing TMSAla instead of Leu[13]. To our best knowledge, this peptide has not been described to date. Peptide **15** represents the N-terminally methylated congener of **14** and in **16** Tyr[11] is additionally replaced by *β,β*-dimethyl-Tyr (**16a**: *β,β*-dimethyl-L-Tyr, **16b**: *β,β*-dimethyl-D-Tyr). Finally, **17**, representing the precursor for fluorescence labeling, contains the N^{α}-methylated, amino-functionalized N^{ω}-carbamoylated arginine in position 8, *β,β*-dimethyl-L-Tyr (**17a**) or *β,β*-dimethyl-D-Tyr (**17b**) in position 11, and TMSAla in position 13 (note: the amino acid positions in the synthesized hexapeptides were assigned with the numbers corresponding to the respective amino acid positions in NT(8−13)). For **14** and **17**, the solid-phase synthesis is exemplarily illustrated in Scheme 1C. Regarding the separation of the diastereomers **16a** and **16b** as well as **17a** and **17b**, this could be conveniently achieved by achiral preparative RP-HPLC. The assignment of the absolute configuration to *β,β*-dimethyl-Tyr in **16a**−**17b** was carried out as recently reported for structurally related NT(8−13) derivatives.[16] This approach is based on NT(8−13) analogs also containing *β,β*-dimethyl-L-Tyr or *β,β*-dimethyl-D-Tyr in position 11, for which the configuration was assigned using CD spectroscopy (structures shown in Figure S1A).[21] As described by Ertl et al.,[16] the elution order in RP-HPLC and the NTS_1R binding affinities served as criteria for the assignment. Derivatives containing *β,β*-dimethyl-L-Tyr consistently elute first (RP-HPLC) and show markedly higher NTS_1R binding affinities compared to the analogs containing *β,β*-dimethyl-D-Tyr (see Figure S1).

The fluorescently labeled peptides **19** and **21** were obtained by treatment of the precursor **17a** with the succinimidyl ester of the 5-TAMRA dye (**18**) or sulfo-Cy5 dye (**20**) in the presence of a base (Scheme 2). The fluorophores were chosen based on different criteria. Both dyes are commercially available at low to moderate costs and filter sets matching the excitation and emission wavelengths of these dyes are available for most instruments used for fluorescence detection. A favorable feature of the 5-TAMRA dye is its high photostability,[25] whereas the sulfo-Cy5 dye is excitable at higher wavelengths (>600 nm) which is advantageous with

https://doi.org/10.1021/acs.jmedchem.5c01701
J. Med. Chem. XXXX, XXX, XXX−XXX

Scheme 1. Structures of the Unnatural Amino acids 10−13, Sequences of the Synthesized Peptides 6 and 14−17b, and Exemplary Schematic Presentation of the Syntheses of 14 and 17[a]

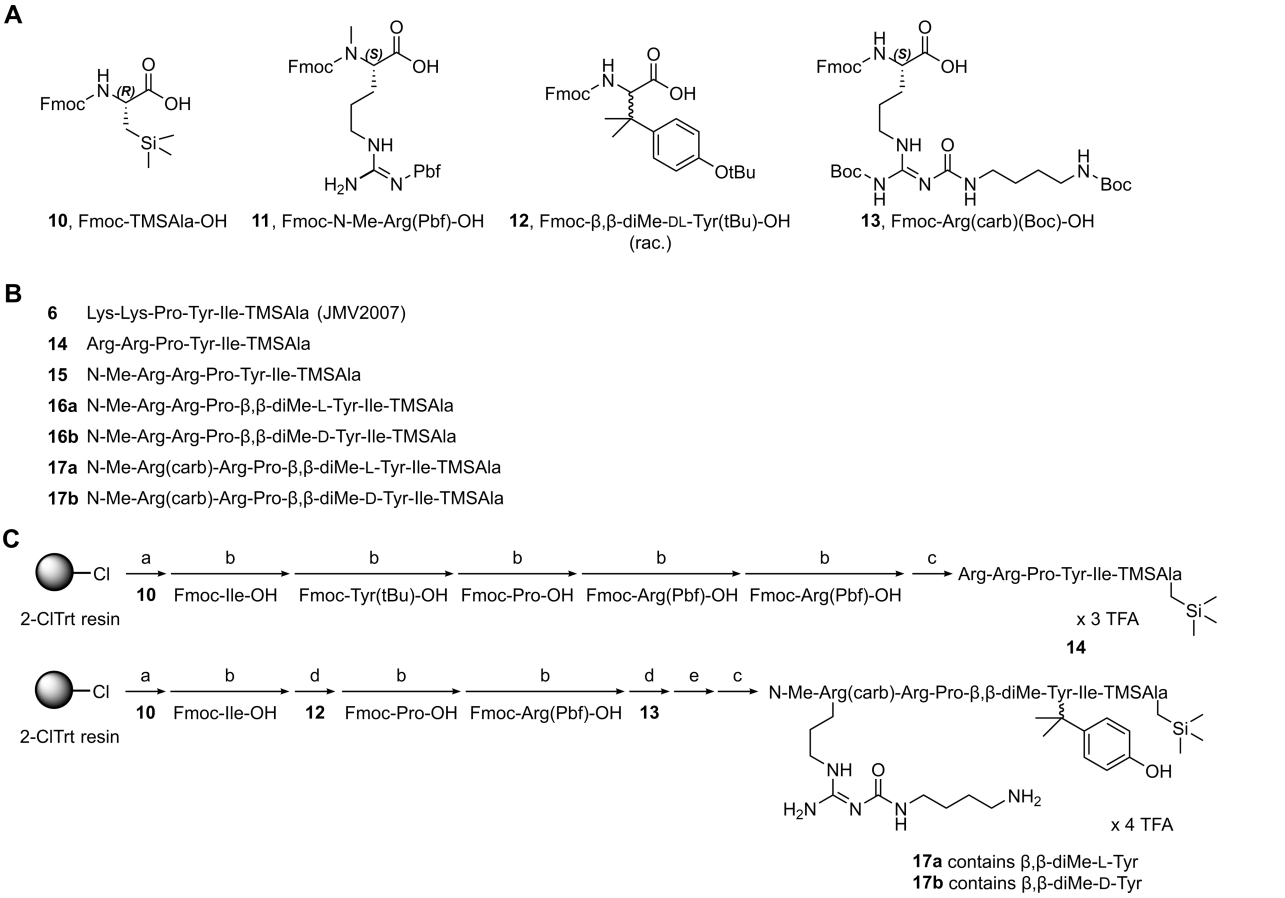

[a](A) Structures of used unnatural amino acids. (B) Amino acid sequences of the synthesized NT(8−13) derivatives. Overall yields for SPPS: 13−52%. (C) SPPS shown for **14** and **17**. Reagents and conditions: (a) anchoring of **10** to a 2-ClTrt resin: **10**/DIPEA (1/2.5 equiv), CH_2Cl_2, rt, overnight, Fmoc deprotection: 20% piperidine in DMF/NMP 8:2 v/v, rt, 2 × 10 min; (b) amino acid coupling: Fmoc-amino acid/HOBt/HBTU/DIPEA (5/5/4.9/10 equiv), DMF/NMP 8:2 v/v, 35 °C, 2 × 45 min ("double" coupling), Fmoc deprotection: as under (a); (c) (1) TFA/CH_2Cl_2 1:3 v/v, rt, 2 × 20 min; (2) TFA/H_2O 95:5 v/v, rt, 5 h; (d) **12** or **13**/HOBt/HBTU/DIPEA (3/3/2.95/6 equiv), DMF/NMP 8:2 v/v, 35 °C, 16 h ("single" coupling), Fmoc deprotection: as under (a); (e) N-terminal methylation according to reported procedures:[21,24] (1) 2-nitrobenzenesulfonylchloride/collidine (3/5 equiv), CH_2Cl_2, rt, 2 h; (2) MTBD/methyl-4-nitrobenzenesulfonate (4/5 equiv), DMF, rt, 30 min; (3) DBU/2-mercaptoethanol (5/10 equiv), DMF, rt, 30 min. The separation of the diastereomers **17a** and **17b** was performed by achiral preparative RP-HPLC. The wavy bond in **17a/b** indicates either configuration, L or D.

respect to an application at cells and tissues. Moreover, both dyes contain a negatively charged acid function conveying increased polarity and solubility.

Chemical and Proteolytic Stability. The chemical stability of the fluorescently labeled ligands **19** and **21** was studied in phosphate-buffered saline (PBS, pH = 7.4) at room temperature over 48 h. Both compounds showed excellent stability (Figures S2 and S3). In the case of **21**, adsorption of the fluorescent ligand to the vessel (visible by eye) resulted in a moderate decrease (ca. 33%) in peptide concentration over 48 h (cf. Figure S3). The adsorption as the cause for the decrease in concentration is also supported by the fact that no additional peak was observed in the RP-HPLC chromatograms. The proteolytic stability of **15**, **17a**, **19**, and **21** was investigated in human plasma at 37 °C over 48 h. NT(8−13), studied as a control, showed very low plasma stability (complete degradation after 30 min, Table 1). The NT(8−13) analog **15**, being N-terminally methylated and containing TMSAla instead of Leu[13] (cf. Scheme 1B), showed moderate proteolytic stability (ca. 50% intact peptide after 48 h). In contrast, the labeling precursor **17a** and the fluorescent ligands **19** and **21**, containing *β,β*-dimethyl-L-Tyr in position 11, exhibited high proteolytic stability (Table 1). The apparent low degradation of peptide **21** (10% after 48 h) can be attributed to the adsorption of **21** to the vessel material as also observed in the case of stability studies in PBS (discussed above). These results show that replacement of Leu[13] by TMSAla as the only C-terminal modification in the NT(8−13) sequence is not sufficient to achieve high proteolytic stability. Consequently, the results confirm that N-terminal methylation in combination with the incorporation of *β,β*-dimethyl-Tyr in position 11 is highly effective in terms of proteolytic stability of NT(8−13) derivatives.

Neurotensin Receptor Binding Studied in Radiochemical Competition Binding Assays. NTS_1R binding affinities were determined in a radioligand competition binding assay as reported[12] using intact HT-29 colon carcinoma cells which express NTS_1R endogenously but no NTS_2R.[12] The tritium-labeled NT(8−13) analog [^{3}H]UR-MK300 (structure shown in Figure S4) was used as radioligand. The obtained K_i

https://doi.org/10.1021/acs.jmedchem.5c01701
J. Med. Chem. XXXX, XXX, XXX−XXX

Scheme 2. Synthesis of the Fluorescently Labeled Peptides 19 and 21[a]

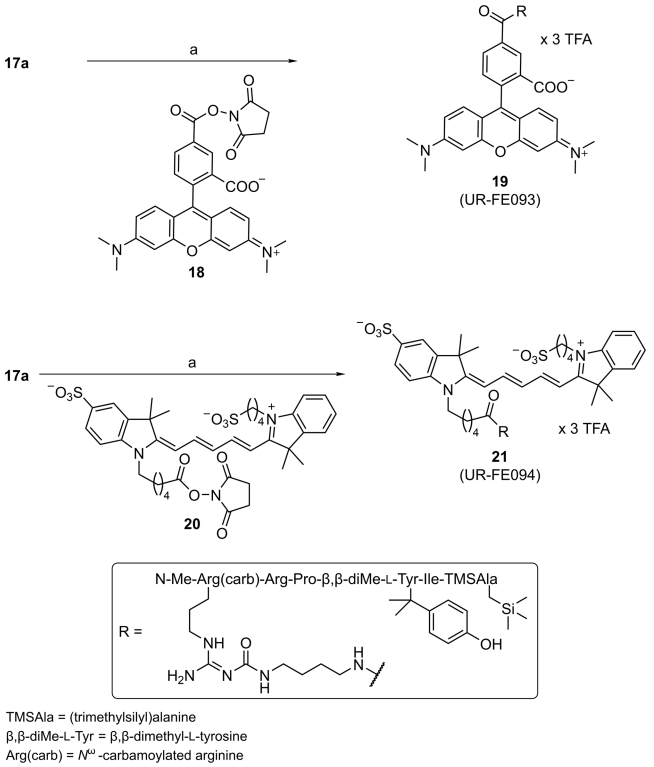

[a]Reagents and conditions: (a) DIPEA, DMF/NMP 8:2 v/v, rt, 1 h; 40% (**19**), 30% (**21**).

values of **6**, **14**-**17b**, **19**, and **21** are presented in Table 2 and competition binding curves are shown in Figure S5A. The previously described peptide **6**, containing two lysines, exhibited high NTS_1R binding affinity with a K_i value of 0.055 nM (Table 2) confirming the reported high binding affinity (IC_{50} = 0.02 nM[19]). Peptide **14**, containing TMSAla instead of Leu[13] as the only structural difference compared to NT(8−13), displayed similar binding affinity as **6**. This confirmed the former observation that replacement of Arg[8] and Arg[9] by Lys[8] and Lys[9] does not affect NTS_1R binding.[20,26−29] N-methylation of **14** (peptide **15**) had no impact on NTS_1R binding as shown in Table 2. This finding is consistent with a previously reported N^{α}-methyl scan of NT(8−13).[22] Replacement of Tyr[11] by β,β-dimethyl-L-Tyr in **15**, resulting in **16a**, did also not affect binding to the NTS_1R (K_i of **16a**: 0.050 nM). Likewise, replacement of Arg[8] in **16a** by the amino-functionalized N^{ω}-carbamoylated arginine (peptide **17a**) did not influence the NTS_1R binding affinity (K_i of **17a**: 0.055 nM). As stated before, the peptides containing β,β-dimethyl-D-Tyr (**16b** and **17b**) showed markedly lower binding affinities (Table 2). The fluorescently labeled peptides **19** and **21**, bearing a bulky fluorescent dye at the side chain of Arg[8], exhibited only slightly higher K_i values (K_i = 0.14 and 0.094 nM, respectively) compared to the precursor **17a**. This confirms that conjugation of NT(8−13) derivatives *via* an N^{ω}-carbamoylated arginine, incorporated in position 8, is a favorable approach in terms of preserving high NTS_1R binding affinity. As a consequence, **19** and **21** bind to the NTS_1R with similar binding affinity to NT(8−13) (K_i = 0.093 nM).

In addition to NTS_1R binding, NTS_2R binding affinities were determined for the fluorescent ligands **19** and **21** in a radiochemical competition binding assay using membranes of HEK293T-hNTS$_2$R cells[21] and [^{3}H]UR-MK300 as radioligand (competition binding curves see Figure S5B). With pK_i values of 9.11 and 9.14, respectively, both probes bind with slightly lower affinity to NTS_2R than to NTS_1R (Table 2).

NTS_1R Agonism. The agonistic potencies of NT(8−13) and the fluorescently labeled NTS_1R ligands **19** and **21** were determined in a Fura-2 Ca^{2+} assay using HT-29 cells (concentration−response curves shown in Figure S6). Peptides **19** and **21** proved to be full agonists with potencies comparable to that of NT(8−13) (Table 2). The pEC_{50} values were consistently circa one log unit lower than the corresponding pK_i values, which can be explained by the nonequilibrium conditions in the case of the Fura-2 Ca^{2+} assay: as the signal occurs immediately after addition of the agonist, the receptor occupancy at the time of the readout is considerably lower than the hypothetical receptor occupancy that would be achieved in equilibrium for the respective concentrations of receptor and receptor ligand. An impairment of the optical readout of the assay by the 5-TAMRA label, whose absorption spectrum (λ_{max} = 555−558 nm, cf. Table 3) largely overlaps with the emission spectrum of the Fura-2 Ca^{2+} complex (λ_{max} = 505 nm),[30] can be excluded based on the results of previous studies using a 5-TAMRA dummy ligand.[31]

Photophysical Characterization. The absorption of the first electronic transition and the emission spectrum of both compounds are their corresponding mirror images indicating a rather constrained molecular scaffold both in the electronic ground and first excited state (Figure S7A,C). However, in the presence of BSA (1% w/w) the spectral distributions shift. In the case of **19**, the spectra blue-shift, while in the case of **21** the spectra red-shift. This already indicates an interaction with the protein's surface. Further, while in the case of **21** the excitation spectrum always resembles the corresponding absorption spectrum with or without BSA, the excitation spectrum of **19** recorded in the absence of BSA already shows a blueshift compared to the corresponding absorption spectrum. This

Table 1. Stabilities of NT(8−13), 15, 17a, 19, and 21 in Human Plasma/PBS 1:2 v/v (37 °C)

	% intact compound in plasma after the specified incubation times[a]					
compd.	10 min	30 min	2 h	6 h	24 h	48 h
NT(8−13)	17 ± 1	<1	<1	<1	n.d.	n.d.
15	n.d.	n.d.	83 ± 1	80 ± 1	65 ± 1	47 ± 1
17a	n.d.	n.d.	>99	>99	>99	>99
19	n.d.	n.d.	>99	95 ± 2	93 ± 2	97 ± 1
21	n.d.	n.d.	97 ± 1	93 ± 1	90 ± 1	90 ± 2

[a]The initial concentration of the peptide in human plasma/PBS (1:2 v/v) was 80 μM. Data represent mean values ± SEM from two or three independent experiments (SEM not given when no degradation was observed).

https://doi.org/10.1021/acs.jmedchem.5c01701
J. Med. Chem. XXXX, XXX, XXX−XXX

Table 2. NTS_1R Binding Affinities of NT(8−13), 6, 14-17b, 19, and 21, and NTS_1R Agonistic Potencies and NTS_2R Binding Affinities of 19 and 21

	NTS_1R		NTS_2R
compd.	$pK_i \pm SEM/K_i$ [nM][a]	$pEC_{50} \pm SEM/EC_{50}$ [nM][b]	$pK_i \pm SEM/K_i$ [nM][c]
NT(8−13)	10.03 ± 0.03/0.093	8.96 ± 0.07/1.2	9.23[16]/0.62[16]
6	10.28 ± 0.06/0.055	n.d.	n.d.
14	10.10 ± 0.02/0.079	n.d.	n.d.
15	10.43 ± 0.1/0.041	n.d.	n.d.
16a	10.30 ± 0.05/0.050	n.d.	n.d.
16b	7.91 ± 0.06/12	n.d.	n.d.
17a	10.39 ± 0.2/0.055	n.d.	n.d.
17b	8.42 ± 0.1/4.2	n.d.	n.d.
19	9.86 ± 0.09/0.14	9.00 ± 0.09/1.1	9.11 ± 0.02/0.78
21	10.04 ± 0.06/0.094	8.89 ± 0.09/1.4	9.14 ± 0.07/0.75

[a]Determined by radioligand competition binding with [^{3}H]UR-MK300[12] at HT-29 colon carcinoma cells. [b]Determined in a Fura-2 Ca^{2+} assay at HT-29 cells. [c]Determined by radioligand competition binding with [^{3}H]UR-MK300[12] at membranes of HEK293T-hNTS_2R cells. Data represent mean values ± SEM (pK_i, pEC_{50}) or mean values (K_i, EC_{50}) from at least three independent experiments performed in triplicate. n.d. not determined.

Table 3. Maxima of the Absorption, Excitation, and Emission Spectra, Fluorescence Lifetimes and Fluorescence Quantum Yields of 19 and 21 in PBS in the Presence or Absence of BSA (1% w/w)

	$\lambda_{abs}/\lambda_{ex}/\lambda_{em}$ [nm]lΔ[eV][a]		τ_{fl} [ns][b]		Φ_{fl} (%)	
compd.	PBS	PBS + 1% BSA	PBS	PBS + 1% BSA	PBS	PBS + 1% BSA
19	558/552/583l0.12	555/553/578l0.097	2.7	3.5	41	34
21	647/648/665l0.049	650/651/669l0.051	1.4	2.7	29	39

[a]Calculated based on λ_{ex} and λ_{em}. [b]Only the main component of a biexponential fit with a contribution >90% is presented.

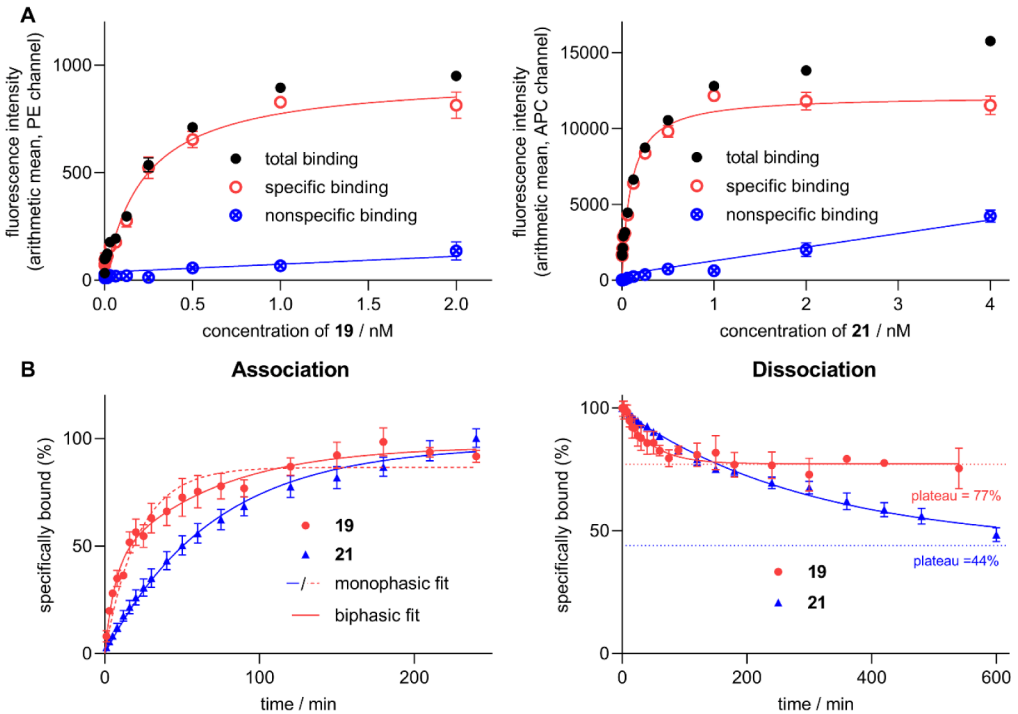

Figure 3. NTS_1R equilibrium binding and kinetic studies of **19** and **21** determined by flow cytometry at intact HT-29 cells. (A) Representative binding isotherms (specific binding, open symbols) of **19** and **21** obtained from saturation binding experiments (incubation: 120 min at 23 °C). Nonspecific binding was determined in the presence of 1 μM NT(8−13). K_d values are presented in Table 4. Data represent mean values ± SEM (total and nonspecific binding) or calculated values ± propagated error (specific binding) from a representative experiment performed in triplicate. (B) Association and dissociation of **19** and **21** studied at 23 °C. Concentrations of **19** and **21** used for the association: 1 nM and 0.1 nM, respectively; concentrations of **19** and **21** used for the preincubation period (**19**: 120 min, **21**: 180 min) of dissociation experiments: 1 nM and 0.25 nM, respectively. Dissociation and association rate constants are presented in Table 4. Data represent mean values ± SEM from at least three independent experiments performed in triplicate.

https://doi.org/10.1021/acs.jmedchem.5c01701
J. Med. Chem. XXXX, XXX, XXX−XXX

Table 4. NTS_1R Binding Data of 19 and 21 Determined by Flow Cytometry at HT-29 and CHO-$hNTS_1R$ Cells

	saturation binding		binding kinetics (HT-29 cells)			
	apparent K_d [nM]					
compd.	HT-29 cells	CHO-$hNTS_1R$ cells	k_{obs} [min^{-1}]	k_{on} [$nM^{-1}min^{-1}$][a]	k_{off} [min^{-1}]	K_d(kin) [nM][b]
19	0.11 ± 0.04	1.2 ± 0.3[c]	$k_{obs,mono}$ = 0.039 ± 0.005	$k_{on,mono}$ = 0.017 ± 0.01	0.021 ± 0.007	1.2 ± 1.3
		0.034 ± 0.009[d]	$k_{obs(bi,fast)}$ = 0.19 ± 0.03	$k_{on(bi,fast)}$ = 0.16 ± 0.04		0.13 ± 0.07
		0.88 ± 0.1[c]	$k_{obs(bi,slow)}$ = 0.016 ± 0.003	$k_{on(bi,slow)}$ = −0.0055 ± 0.01		n.a.
21	0.046 ± 0.02	0.022 ± 0.005[d]	0.014 ± 0.002	0.11 ± 0.02	0.0033 ± 0.0002	0.030 ± 0.007

[a]Association rate constant ± propagated error calculated from k_{off}, k_{obs}, and the ligand concentration used for the association experiments. [b]Kinetically derived dissociation constant ± propagated error calculated from k_{off} and k_{on} values. K_d, k_{obs}, and k_{off} values represent mean values ± SEM from at least three independent experiments; k_{on} and K_d(kin) values represent calculated values ± propagated error. [c]Experiments performed with a cell density of 150,000 cells/mL. [d]Experiments performed with a cell density of 15,000 cells/mL. n.a. not applicable.

indicates a significant structural rearrangement of the molecular framework in the excited state compared to the ground state. The impact of BSA in form of interactions to the chromophore is further manifested in altered fluorescence quantum yields and lifetimes (Table 3). Each chromophoric system shows a prolonged excited singlet state lifetime in the presence of BSA. To note, the emission decay is biexponential and the second lifetime is of small amplitude (cf. Figure S7B,D), which may arise either from small impurities or an equilibrium between different conformers. Interestingly, while **19** shows a decreased fluorescence quantum yield, **21** shows an increased fluorescence quantum yield. In the case of **19**, this may indicate a deactivation process induced by the interaction with the protein. An electron transfer from a redox active amino acid to the chromophore or the hindrance for structural changes in the excited state, which could result in a brighter emissive configuration, may represent two potential explanations. This will be addressed by transient absorption spectroscopy and presented elsewhere. In the case of **21**, the emissive character of the electronically excited chromophore is apparently inversely effected. Here, the data suggest a situation in which, in the excited state, the molecule undergoes structural changes forming a less emissive configuration that is hindered when attached to the protein's surface. Also, in this case the transient absorption will inform on the mechanistic scenario in more detail, which will be presented elsewhere. The observed changes in quantum yield are in accordance with reported studies on 5-TAMRA-labeled and sulfo-Cy5-labeled fluorescent GPCR ligands.[13,31−33]

Investigation of NTS_1R Binding of 19 and 21 by Flow Cytometry. The flow cytometric binding experiments were carried out at 23 °C using a BD FACSCanto II cytometer equipped with an argon laser (488 nm) and a red laser (640 nm). Saturation binding experiments with **19** and **21** were performed at live human HT-29 colon carcinoma cells and stably transfected CHO-$hNTS_1R$ cells. For both ligands, specific binding was saturable (Figures 3A and S8), however, the apparent K_d values determined at CHO-$hNTS_1R$ cells were higher (10−20-fold) compared to the apparent K_d values obtained from HT-29 cells (Table 4) which were in good agreement with the K_i values determined by competition binding with [^{3}H]UR-MK300 at HT-29 cells (Table 2). The higher K_d values determined at CHO-$hNTS_1R$ cells can be explained by the markedly higher NTS_1R expression in CHO-$hNTS_1R$ cells (ca. 300,000 receptors/cell) compared to HT-29 cells (ca. 45,000 receptors/cell).[12] As the studied ligands **19** and **21** show subnanomolar binding affinities, a high receptor concentration in saturation binding experiments leads to ligand depletion and consequently results in higher apparent K_d values.[34] This effect can be reduced by using less cells in the experiment. Typically, for this kind of flow cytometric analysis, cell densities ≥100,000 cells/mL are used to obtain a reasonable number of gated events (≥2000), required for the calculation of representative fluorescence intensity mean values, within a reasonable measuring time. To explore the influence of the receptor concentration and associated with this the effect of ligand depletion on the discrepancy between the apparent K_d and the true K_d, additional saturation binding experiments were performed with CHO-$hNTS_1R$ cells using a considerably lower cell density of 15,000 cells/mL. These conditions resulted in 200−300 gated events, just high enough to enable a statistically reasonable data analysis. The apparent K_d values of **19** and **21** obtained from these saturation binding experiments were markedly lower (factor > 10) than the apparent K_d values obtained from saturation binding studies using 150,000 cells/mL (Table 4 and Figure S8) and similar to the K_d values determined at HT-29 cells. The apparent K_d values determined at low receptor concentrations (HT-29 cells, CHO-$hNTS_1R$ cells at a density of 15,000 cells/mL) should better resemble the true K_d, although the latter is potentially even lower than the experimentally determined dissociation constants.

Noteworthy, the excitation laser line (640 nm) used for the excitation of the sulfo-Cy5 dye in **21** is close to its absorption maximum (647/650 nm, see Table 3). In contrast, the excitation of the 5-TAMRA label in **19** by the 488 nm argon laser is not ideal with respect to its absorption maximum (558/555 nm, Table 3). This is also reflected by the markedly lower B_{max} values obtained from saturation binding experiments with **19** compared to **21** (Figure 3A).

Kinetic binding studies, performed at HT-29 cells, revealed notable differences between **19** and **21**. While **21** showed a monophasic association, the 5-TAMRA-labeled ligand **19** displayed a clear biphasic association (two-phase association favored over one-phase association according to the *F*-test, $P < 0.005$, GraphPad Prism 5) (Figure 3B). The proportion of the fast and slow association phase was 42:58 (based on the fit to the data shown in Figure 3B). The observed association rate constants k_{obs} and the calculated association rate constants k_{on} are shown in Table 4. The $k_{on(bi,slow)}$ value, calculated from $k_{obs(bi,slow)}$, k_{off}, and the concentration of **19** used for the association studies, was negative. This could be due to internalization of ligand−receptor complex during the association process (cf. Figure 6), but could also be attributed to the low ratios of total over nonspecific binding in the case of **19** particularly during the initial phase of the association (discussed in more detail below). As the $k_{on(bi,slow)}$ was negative, precluding a calculation of the kinetically derived

https://doi.org/10.1021/acs.jmedchem.5c01701
J. Med. Chem. XXXX, XXX, XXX−XXX

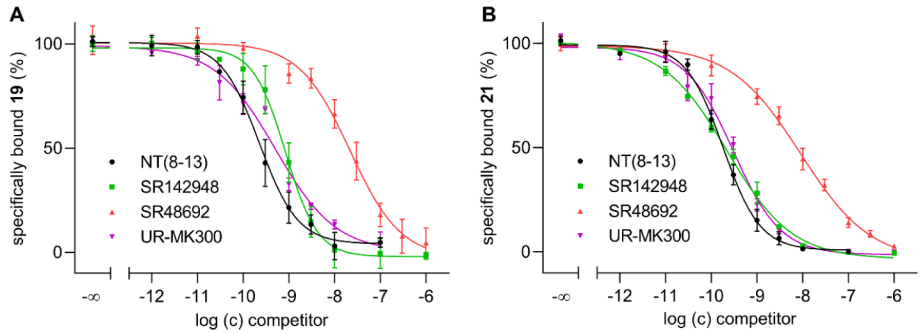

Figure 4. Displacement curves from flow cytometric competition binding studies using **19** (A) or **21** (B) as a labeled probe and NT(8−13), SR142948, SR48692, or UR-MK300 as competitors. Experiments were performed at intact HT-29 cells at 23 °C. The concentrations of **19** and **21** were 0.3 nM and 0.1 nM, respectively. Incubation times: 120 min (A) and 180 min (B). Data represent mean values ± SEM from at least three individual experiments performed in triplicate.

dissociation constant K_d(kin), the association data of **19** were additionally fitted with a monophasic exponential fit covering the whole association process. This enabled the calculation of a K_d(kin) value which comprises the entire association (see below).

The fact that one ligand shows a monophasic and the other ligand a biphasic association for the same cellular system suggests that the biphasic association cannot be explained by the existence of two subpopulations of NTS_1R (e.g., one coupled to and the other uncoupled from G-protein). It should be mentioned that for the association studies of **19**, a fluorescent ligand concentration corresponding to 9-fold the K_d value of **19** had to be used since with lower ligand concentrations, correlating with lower receptor occupancies, the difference between total and nonspecific binding was too low for a reliable data analysis. This was particularly due to the aforementioned mismatch of the excitation wavelength and the absorption maximum of the 5-TAMRA dye in **19**. In contrast, for association studies with **21**, a ligand concentration corresponding to 3-fold the K_d value could be used because of the optimal excitation of the sulfo-Cy5 dye in **21** with the red laser (640 nm) resulting in the detection of high fluorescence intensities. It is noteworthy that, in the case of experiments with **19**, the excitation with 488 nm light gave a high autofluorescence of the cells which also affected data analysis. The excitation of the cells with 640 nm (used for **21**) resulted in very low autofluorescence. The different ligand concentrations used for the association experiments might be the reason for the observed differences in the association kinetics of **19** and **21** (biphasic vs monophasic). Moreover, it could be explained by the internalization of ligand−receptor complex (as confirmed by confocal microscopy, see below), occurring already during the association process. Upon internalization, ligand-dependent differences could occur with respect to changes of fluorescent properties in the cell interior and retrafficking of ligand−receptor complex or free receptor to the plasma membrane.

Dissociation studies at HT-29 cells, initiated by adding an excess of NT(8−13), gave monophasic dissociation curves revealing an incomplete dissociation (plateau significantly higher than zero, $P < 0.05$, t-test) as also previously reported for fluorescently labeled NT(8−13) derivatives.[13,16] The plateau values amounted to 77% (**19**) and 44% (**21**). This can be explained by the NTS_1R agonism of **19** and **21** (cf. Figure S6) meaning that the ligand−receptor complex is internalized, potentially followed by intracellular dissociation of the fluorescent ligand from the receptor. The k_{off} values of **19** and **21** differed by a factor of 7 (k_{off} = 0.021 min^{-1} vs 0.0033 min^{-1}, see Table 4). Compared to previously described fluorescently labeled NT(8−13) derivatives, **19** and **21** show a slower dissociation from NTS_1R which is favorable for imaging of NTS_1R expression in cells or tissues. The kinetically derived dissociation constants K_d(kin) (Table 4) were calculated according to K_d(kin) = k_{off}/k_{on}. In the case of **19**, the K_d(kin) was calculated from $k_{on,mono}$ and $k_{on(bi,fast)}$ yielding K_d(kin) values of 1.2 and 0.13 nM, respectively. The value of 0.13 nM is in excellent agreement with the K_d obtained from saturation binding (Table 4). Likewise, the K_d(kin) value obtained for **21** is in good agreement with the K_d from saturation binding studies (0.030 nM vs 0.046 nM), indicating a binding process largely following the law of mass action. Yet, the determined kinetic parameters of **19** and **21** must be interpreted with care since both ligands induce receptor endocytosis (cf. Figures 6 and 7) and show an incomplete dissociation. Moreover, as discussed before, flow cytometric kinetic studies with the 5-TAMRA-labeled ligand **19** were compromised by the non-optimal excitation and higher autofluorescence compared to **21**.

To investigate the suitability of **19** and **21** to serve as probes for the determination of NTS_1R binding affinities of unlabeled NTS_1R ligands, the K_i values of reported NTS_1R ligands (NT(8-13), SR142948, SR48692, UR-MK300) were determined in flow cytometric competition binding studies at HT-29 cells using **19** or **21** as labeled probe (displacement curves shown in Figure 4).

Although the dissociation kinetics of **19** and **21**, indicating long-lasting binding, is not ideal in terms of competition binding experiments, the pK_i values obtained for the reference ligands were generally in good agreement with reported data (Table 5).

The Hill coefficients of the displacement curves (4-parameter logistic fit) were not significantly different from −1 (two-tailed t test, $P > 0.05$) except for SR142948 and SR48692 studied with **21** (Hill coefficients: −0.63 ± 0.02 and −0.55 ± 0.06, respectively; mean values ± SEM). The low slope factors might be attributed to the (pseudo)irreversible binding of **21** (cf. Figure 3B) or to the internalization and putative externalization of NTS_1R induced by the fluorescent agonists, potentially resulting in a retarded displacement of fluorescent ligand. However, for the other competitors (NT(8−13), MK300) and for all competitors studied with **19**, also showing (pseudo)irreversible binding, the Hill

https://doi.org/10.1021/acs.jmedchem.5c01701
J. Med. Chem. XXXX, XXX, XXX−XXX

Table 5. NTS_1R Binding Affinities of Reported NTS_1R Ligands Determined by Flow Cytometry at HT-29 Cells Using 19 and 21 as Labeled Probes[a]

	pK_i		
compound	19	21	literature
NT(8−13)	10.20 ± 0.2	10.25 ± 0.09	9.85,[12] 9.62,[28] 9.54,[35] 9.00,[18] 9.55,[16] 10.09[16]
SR142948	9.70 ± 0.1	10.14 ± 0.08	8.96,[12] 9.24,[16] 9.74,[16] 9.00[36]
SR48692	8.25 ± 0.1	8.49 ± 0.2	8.07[37]
UR-MK300	9.85 ± 0.1	10.05 ± 0.1	9.33[12]

[a]Reported K_i values were converted to pK_i values. Data represent mean values ± SEM from at least three individual experiments performed in triplicate.

coefficients were not significantly lower than unity, which contradicts the aforementioned hypothesis. Since slope factors different from unity could also arise from the existence of ligand-dependent multiple conformational receptor states,[38,39] the low slopes observed for SR142948 and SR48692 could be caused by the preference of different receptor conformations of the used NTS_1R ligands: whereas the agonist **21** prefers the active conformation, the antagonists do not discriminate between receptor states or even prefer the inactive conformation.[40,41]

Cooperativity between 21 and the Allosteric NTS_1R Modulator SBI-553. In recent years, several allosteric NTS_1R modulators, targeting an intracellular binding site, have been reported.[42−45] *In vivo* studies suggested that allosteric potentiators of NTS_1R binding of neurotensin can potentially be used as therapeutics for the treatment of pain.[45] A prominent example is the positive allosteric modulator SBI-553 which was demonstrated to potentiate binding of radiolabeled neurotensin or NT(8−13).[42,44] To explore if SBI-553 also enhances binding of fluorescently labeled NT(8−13) derivatives such as **21**, the effect of SBI-553 on NTS_1R binding of **21** was studied by flow cytometry using HT-29 tumor cells. For these experiments, **21** was used at a concentration of 0.01 nM, corresponding to approximately one-fifth of its K_d, and these samples were titrated with SBI-553. As previously observed in the radiochemical assays,[42,44] SBI-553 clearly enhanced NTS_1R binding of **21** (Figure 5). However, in contrast to the reported studies, a biphasic CEC of SBI-553 was obtained, yielding a pEC_{50}(high) of 10.37 and a pEC_{50}(low) of 7.28. The latter is in excellent agreement with the reported pEC_{50} value of SBI-553 of 7.30[44] and with the described EC_{50} value of 140 nM.[42] To note, in contrast to the pEC_{50}(low), the pEC_{50}(high) was not well reproducible in the individual experiments which is reflected by the high SEM of 0.40 (cf. Figure 5). The E_{max} observed for SBI-553 (E_{max} = 88%) was lower than the reported E_{max} of 140%[42] and 242%.[44]

It is a matter of speculation why SBI-553 shows a biphasic CEC when studied with the fluorescent ligand **21**. The major differences compared to the reported radiochemical assays[42,44] are the type of labeled ligand (radiolabeled vs fluorescently labeled), the use of intact cells (in contrast to membrane preparations in the reported studies), and a measurement under equilibrium conditions in the present study (flow cytometry). Supposedly, the biphasic course of the CEC of SBI-553 can be attributed to one or more of these differences in the technical setup of the binding assays. The elucidation of the underlying mechanisms requires further studies. Likewise,

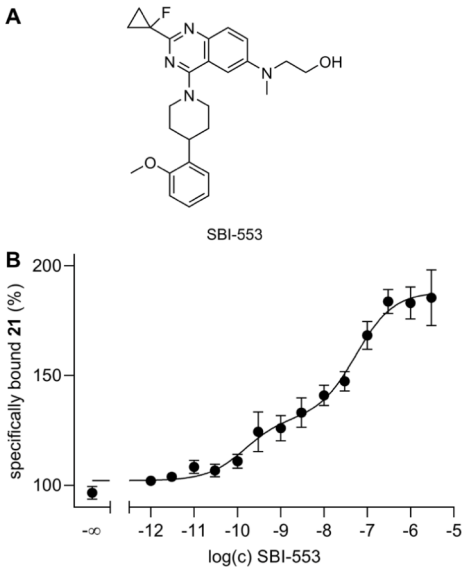

Figure 5. (A) Structure of the allosteric NTS_1R modulator SBI-553. (B) Effect of SBI-553 on NTS_1R binding of the fluorescent NT(8−13) derivative **21** (c = 0.01 nM) determined in a flow cytometric binding assay performed with intact HT-29 cells at 23 °C. Cells were preincubated with SBI-553 for 30 min prior to the addition of **21** and continued incubation for 180 min. SBI-553 enhanced binding of **21** in a biphasic manner (fraction high/low: 0.33/0.67). 100% specifically bound **21** corresponds to specific binding of **21** in the absence of SBI-553. Data represent mean values ± SEM from six individual experiments performed in triplicate. pEC_{50}(high) = 10.37 ± 0.40. pEC_{50}(low) = 7.28 ± 0.16. E_{max} = 88 ± 8% (difference between lower and upper plateau).

the lower E_{max} compared to the reported E_{max} values[42,44] could also arise from the different assay parameters.

Confocal Microscopy. Binding of **19** and **21** to both HT-29 cells, natively expressing NTS_1R, and stably transfected CHO-hNTS_1R cells, overexpressing the NTS_1R, was studied by confocal microscopy at 22 °C using a confocal laser scanning microscope. In all cases, a marked difference between total and nonspecific binding was found (Figures 6 and 7; Figures S9 and S10), showing that the NTS_1R expression can be visualized with both fluorescent ligands, even at low receptor expression levels (HT-29 cells, Figures 6 and 7).

The excitation with 561 nm (**19**) resulted in higher autofluorescence compared to an excitation with 633 nm (**21**). This was only observable when using HT-29 cells (cf. Figures 6D and 7D) because the lower receptor expression in these cells compared to CHO-hNTS_1R cells (cf. Figures S9D and S10D) necessitates higher laser power and higher detector gain (see Experimental Section). As becomes obvious from Figures 6C and 7C, showing nonspecific binding of **19** and **21**, respectively, the 5-TAMRA-labeled ligand **19** exhibited considerably higher nonspecific binding compared to the sulfo-Cy5-labeled probe **21**.

The microscopic studies with **19** and **21** revealed that the NTS_1R is internalized by endocytosis upon binding of the fluorescent ligands, occurring already during the association process (Figures 6 and 7; Figures S9 and S10). The intracellular fluorescent ligand appeared to be located in vesicles. The internalization rates were estimated by defining an outer ROI, representing the total cellular fluorescence, and an inner ROI, representing the intracellular fluorescence, and quantification of fluorescence (Figure S11). This analysis

https://doi.org/10.1021/acs.jmedchem.5c01701
J. Med. Chem. XXXX, XXX, XXX−XXX

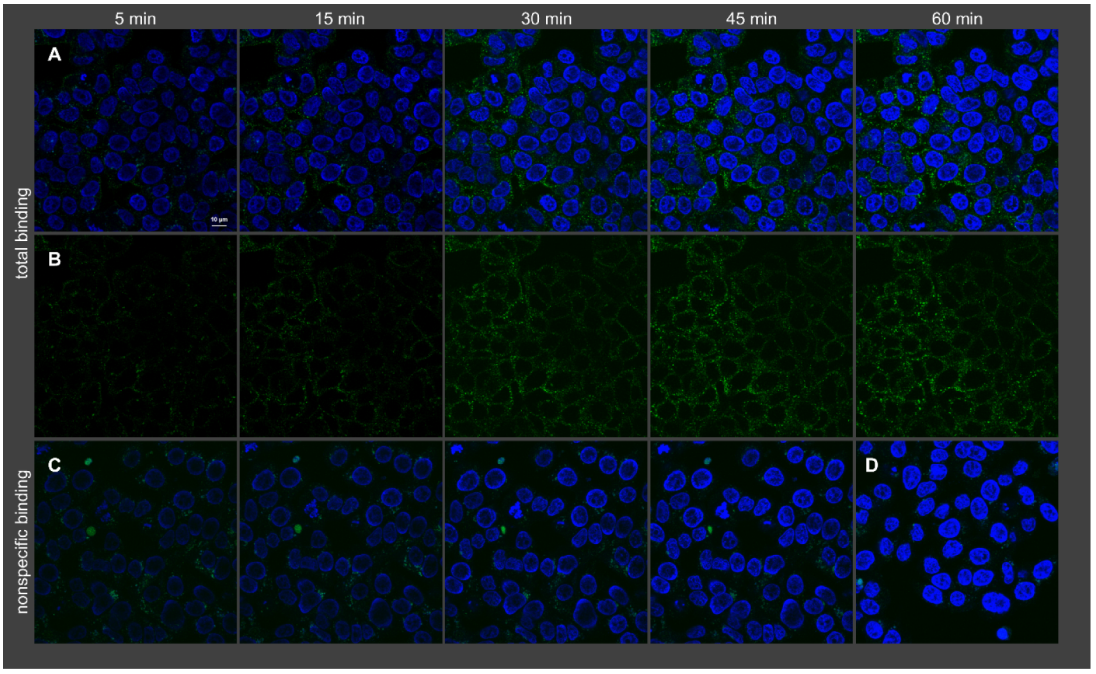

Figure 6. Visualization of binding of **19** (2 nM) to intact HT-29 cells (temperature: 22 °C) by confocal microscopy. Shown is total binding (A, B), nonspecific binding (C), and autofluorescence (D). Nuclei were stained with H33342 (2 μg/mL). (A) Merged fluorescence of **19** (green) and nuclei (blue). (B) Fluorescence of **19**, without nuclei. (C) Merged fluorescence of **19** and nuclei acquired in the presence of 1 μM NT(8−13).

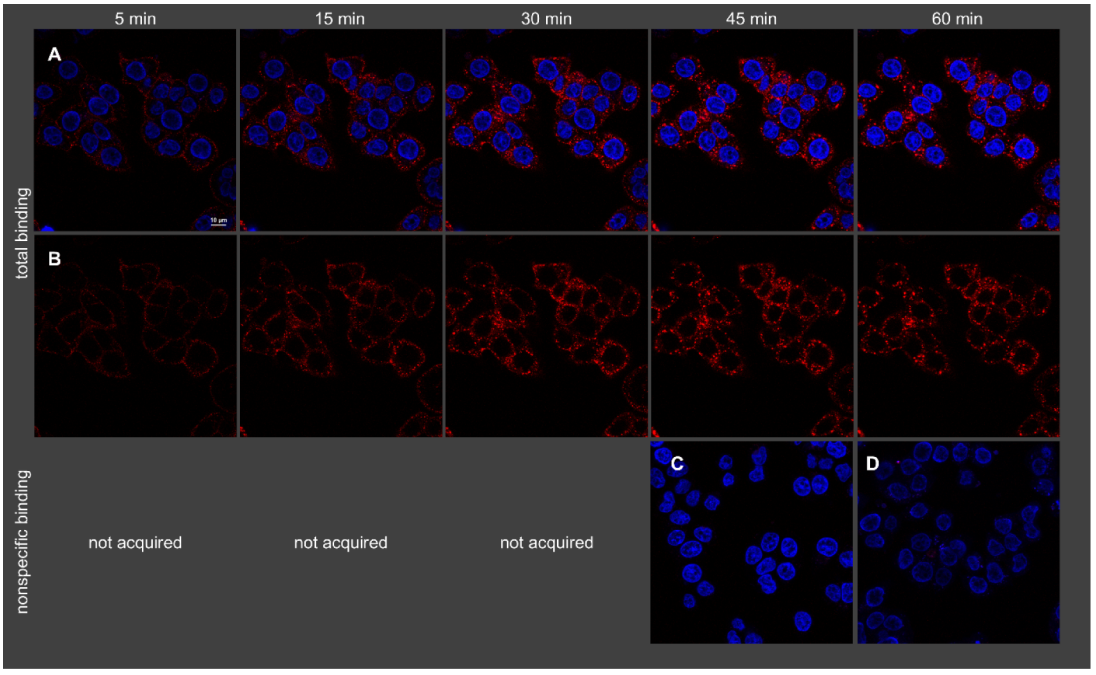

Figure 7. Visualization of binding of **21** (2 nM) to intact HT-29 cells (temperature: 22 °C) by confocal microscopy. Shown is total binding (A, B), nonspecific binding (C), and autofluorescence (D). Nuclei were stained with H33342 (2 μg/mL). (A) Merged fluorescence of **21** (red) and nuclei (blue). (B) Fluorescence of **21**, without nuclei. (C) Merged fluorescence of **21** and nuclei acquired in the presence of 1 μM NT(8−13). Note: as no nonspecific binding of **21** was observed, images of nonspecific binding were only acquired after 45 min.

suggests that the fraction of internalized ligand only slightly increases over the studied time (5−60 min). This could be explained by recycling of NTS_1R to the plasma membrane after internalization as also suggested by previous studies of fluorescently labeled NT(8−13) analogs.[13] It should be noted that the determined internalization rate represents only a rough estimation due to the visual definition of the ROIs and potentially biased fluorescence intensities caused by changes in the photophysical properties of the fluorescent ligands in the intracellular environment.

Biomolecular Imaging of NTS_1R Expression in Cells and Tumor Tissue. In another approach, the suitability of **19** and **21** to serve as probes for the investigation of NTS_1R expression in living cells and tumor tissue was studied using an

https://doi.org/10.1021/acs.jmedchem.5c01701
J. Med. Chem. XXXX, XXX, XXX−XXX

Azure Sapphire Biomolecular Imager. For these experiments, HT-29 cells, showing a low NTS_1R expression,[12] and HT-29 tumors subcutaneously grown in nude mice were used. Saturation binding experiments with the sulfo-Cy5-labeled ligand **21** at adherent HT-29 cells gave satisfactory fluorescence images revealing low nonspecific binding of **21** (Figure 8A). Based on the fluorescence intensities, saturation binding curves could be generated (Figure 8B) yielding a K_d value of 1.7 ± 1 nM (mean value ± SEM from four individual experiments performed in triplicate), which was higher than the K_d value obtained from flow cytometric saturation binding experiments at suspended HT-29 cells (cf. Table 4).

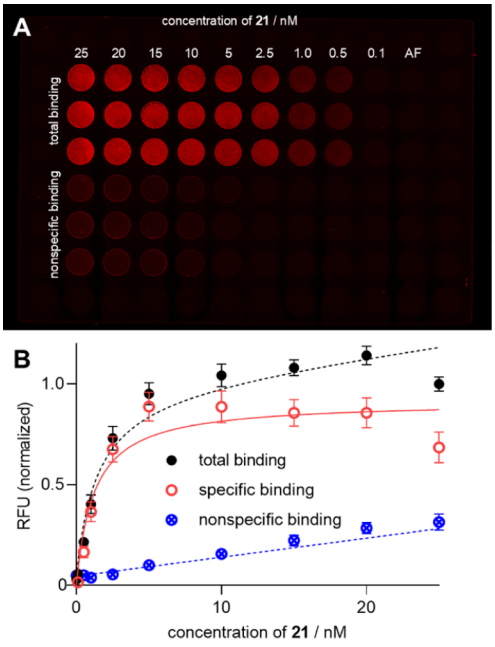

Figure 8. (A) Fluorescence image of a 96-well plate with adherent HT-29 cells acquired with an Azure Sapphire Biomolecular Imager (laser: 658 nm; pixel size: 20 μm) 2 h after incubation with **21** at rt. Nonspecific binding was determined in the presence of SR142948 (1 μM). Shortly before image acquisition, cells were washed three times with cold buffer. (B) Fluorescence intensities from (A) plotted against the concentration of **21**. Specific binding was calculated from total and nonspecific binding. Data represent means ± SEM (total and nonspecific binding) or calculated values ± propagated error (specific binding) from four independent experiments performed in triplicate.

This discrepancy could be explained by a lower sensitivity of the biomolecular imaging technique compared to the flow cytometric analysis, meaning that cell-bound fluorescence is underestimated for low ligand concentrations in the case of biomolecular imaging. Moreover, a higher adsorption of **21** to the plate material (polystyrene) and the required washing step in the case of the biomolecular imaging could account for the higher K_d value compared to the flow cytometric experiment which uses polypropylene plates and allows a measurement under equilibrium conditions (no washing required).

In contrast to **21**, the fluorescence images obtained from the same experiment performed with the 5-TAMRA-labeled ligand **19** were not suited for the determination of a K_d value due to high autofluorescence and high nonspecific binding (Figure S12).

Using the same biomolecular imager, visualization of NTS_1R expression in HT-29 tumors was explored by imaging 10 μm cryosections of tumor tissue after incubation with **19** and **21**. As observed for the saturation binding experiment with HT-29 cells, a detection of NTS_1R expression in the tumor was possible with the red-emitting probe **21** (Figure 9), but failed when using the 5-TAMRA-labeled ligand **19** as probe mainly due to high autofluorescence relative to specific binding (Figure S13). The regions of the tumor sections showing high nonspecific binding of **21** (Figure 9) likely represent necrotic tumor tissue. It should be noted that the HT-29 tumors originated from a former research project and had been stored for more than eight years at −80 °C.[12] This long-term storage might have led to partial unfolding or degradation of the receptor protein.

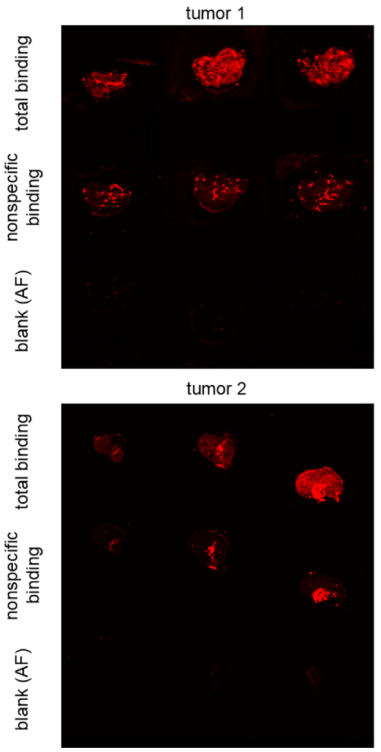

Figure 9. Fluorescence images of cryosections (size: 11−28 mm^2, thickness: 10 μm) of a HT-29 tumor acquired after incubation with **21** (5 nM) at rt for 60 min with an Azure Sapphire FL Biomolecular Imager (laser: 658 nm; pixel size: 20 μm). Nonspecific binding was determined in the presence of SR142948 (5 μM). Blank samples were incubated with neat buffer to determine background signals. Shortly before image acquisition, tumor sections were washed three times with cold buffer.

CONCLUSION

N-terminal methylation and the replacement of Arg^8, Tyr^{11}, and Leu^{13} in NT(8−13) by an amino-functionalized carbamoylated arginine, β,β-dimethyl-L-Tyr, and TMSAla, respectively, resulted in a NT(8−13) analog (**17a**, UR-FE083-I) that was used as a precursor for the preparation of a 5-TAMRA-labeled (**19**, UR-FE093) and a sulfo-Cy5-labeled (**21**, UR-FE094) NTS_1R ligand. Both fluorescent ligands show subnanomolar NTS_1R binding affinities with K_i values of 0.14 nM and 0.094 nM. The high binding affinity allows an application of these probes for flow cytometric binding assays using cells with low NTS_1R expression levels, which was

https://doi.org/10.1021/acs.jmedchem.5c01701
J. Med. Chem. XXXX, XXX, XXX−XXX

demonstrated for nontransfected HT-29 cells natively expressing the NTS_1R.

The fluorescent peptides **19** and **21** display high *in vitro* proteolytic stability ($t_{1/2} \gg 48$ h, human plasma), which is favorable with respect to binding studies in living cells potentially featuring proteolytic activities. **19** and **21** are anticipated to exhibit also high stability *in vivo* since recently described NT(8−13)-derived PET ligands, containing an N-terminal methyl group and *β*,*β*-dimethyl-L-Tyr in position 11, showed high *in vivo* stability in mice.[21]

Fluorescence imaging of receptor expression in tissues represents an attractive alternative to autoradiography that requires radiolabeled receptor ligands. The present study reveals that the 5-TAMRA-labeled ligand **19** is not suited for fluorescence-based imaging of the NTS_1R expression in tumor tissue. This shows that the 5-TAMRA label, although characteristic of high photostability,[25] does not meet the demands for this kind of imaging, in particular due to the excitation wavelength of <600 nm, resulting in interfering autofluorescence. Contrarily, the near-infrared sulfo-Cy5-labeled probe **21**, differing from **19** only with respect to the fluorescent dye, turned out to be an excellent molecular tool for NTS_1R imaging in tumor tissue sections with high signal-to-noise ratio (used excitation: 658 nm), suggesting its application in tumor tissue screening procedures. As **19** and **21** display also high NTS_2R binding affinity, they can potentially serve as probes for NTS_2R binding studies using cellular systems solely expressing NTS_2R.

One of the major challenges with respect to the *in vivo* use of labeled peptidic NTS_1R ligands has been the development of tracers which exhibit both high proteolytic stability and high NTS_1R binding affinity (K_i < 1 nM). With the development of the amine-functionalized precursor **17a**, which can be conjugated to various molecular labels, the present study paved the way to the future synthesis and use of high-affinity and proteolytically stable probes for the NTS_1R with a functionality of choice.

EXPERIMENTAL SECTION

Materials. The protected amino acids Fmoc-Tyr(*t*Bu)−OH, Fmoc-Arg(Pbf)−OH, and glycine *tert*-butyl ester hydrochloride (**22**) were purchased from Carbolution Chemicals (St. Ingbert, Germany). Fmoc-N-Me-Arg(Pbf)−OH (**11**), Fmoc-Lys(Boc)−OH, Fmoc-Pro-OH, Fmoc-Ile-OH, and HBTU were from Merck (Darmstadt, Germany). Racemic Fmoc-*β*,*β*-dimethyl-Tyr(*t*Bu)−OH (**12**) and 2-ClTrt resin were obtained from Iris Biotech (Marktredwitz, Germany). HOBt, 7-methyl-1,5,7-triazabicyclo[4.4.0]dec-5-ene (MTBD), methyl-4-nitrobenzenesulfonate, 2-mercaptoethanol, and 1-methyl-D-Trp were from Sigma-Aldrich (Taufkirchen, Germany). Collidine, 2-nitrobenzenesulfonyl chloride, 1,8-diazabicyclo[5.4.0]undec-7-ene (DBU), NMP and DMF for peptide synthesis, anhydrous DMF and NMP, dichloromethane, piperidine, and TFA were purchased from Fisher Scientific (Schwerte, Germany). (1*R*,2*R*,5*R*)-2-Hydroxy-3-pinanone (**23**) and (iodomethyl)trimethylsilane (**25**) were from TCI (Eschborn, Germany). DIPEA was obtained from ABCR (Karslruhe, Germany). Acetonitrile (HPLC gradient grade) was from VWR (Ismaning, Germany). NT(8−13) was synthesized *via* SPPS in-house. SR142948 and SR48692 were purchased from Tocris Bioscience (Bristol, UK). SBI-553 was from Biocat (Heidelberg, Germany). Bacitracin, HEPES, and bovine serum albumin (BSA) were obtained from Serva (Heidelberg, Germany). Fetal bovine serum (FBS) was purchased from Pan-Biotech (Aidenbach, Germany). Fura-2 AM and Pluronic F-127 were obtained from Calbiochem/Merck Biosciences (Beeston, UK). The radioligand [^{3}H]UR-MK300 (molar activity: 2.41 TBq/mmol) and its unlabeled analog UR-MK300 were prepared according to a described procedure.[12] Compounds **10**[23] and **13**[12] were prepared according to the reported procedures. 5-TAMRA succinimidyl ester (**18**) was purchased from Carl Roth (Karlsruhe, Germany). Sulfo-Cyanine5 NHS ester (S0586, **20**) was obtained from FEW Chemicals (Bitterfeld, Germany). Millipore water was consistently used for the preparation of stock solutions, buffers, and aqueous eluents for HPLC. Polypropylene reaction vessels with screw cap (1.5 or 2 mL) from Sarstedt (Nümbrecht, Germany) were used for small-scale reactions (e.g., activation of Fmoc-protected amino acids) and to keep stock solutions.

NMR Spectroscopy. NMR spectra were recorded on an AVANCE 600 instrument with cryogenic probe (^{1}H: 600 MHz; ^{13}C: 150 MHz) and an AVANCE 400 instrument (^{1}H: 400 MHz; ^{13}C: 100 MHz) (Bruker, Karlsruhe, Germany). NMR spectra were calibrated based on the solvent residual peaks (^{1}H NMR, DMSO-d_6: δ = 2.50 ppm, $CDCl_3$: δ = 7.26 ppm; ^{13}C NMR, DMSO-d_6: δ = 39.50 ppm, $CDCl_3$: δ = 77.16 ppm) and data are reported as follows: ^{1}H NMR: chemical shift δ in ppm (multiplicity [s = singlet, d = doublet, *t* = triplet, *m* = multiplet, br s = broad singlet], integral, coupling constant *J* in Hz); ^{13}C NMR: chemical shift δ in ppm.

Mass Spectrometry. High-resolution mass spectrometry (HRMS) was performed with an Agilent 6540 UHD accurate-mass Q-TOF LC/MS system coupled to an Agilent 1290 analytical HPLC system (Agilent Technologies. Santa Clara, CA) using an ESI source and the following LC method: column: Agilent Zorbax Eclipse Plus C18, 1.8 μm, 50 × 2.1 mm, column temperature: 40 °C, solvent/linear gradient: 0−4 min: 0.1% aqueous HCOOH/acetonitrile supplemented with 0.1% HCOOH 95:5−2:98, 4−5 min: 2:98, flow: 0.6 mL/min.

Preparative HPLC. Preparative HPLC was performed with a system from Knauer (Berlin, Germany) consisting of two K-1800 pumps and a K-2001 detector (in the following referred to as "system 1") or with a Prep 150 LC system from Waters (Eschborn, Germany) comprising a Waters 2545 binary gradient module, a Waters 2489 UV/vis detector, and a Waters fraction collector III (in the following referred to as "system 2"). A Gemini NX-C18, 5 μm, 250 mm × 21 mm (Phenomenex, Aschaffenburg, Germany) was used as stationary phase at a flow rate of 20 mL/min using mixtures of 0.1% aqueous TFA and acetonitrile as the mobile phase. A detection wavelength of 220 nm was used throughout. Collected fractions were lyophilized using a Scanvac CoolSafe 100−9 freeze-dryer (Labogene, Allerød, Denmark) equipped with a RZ 6 rotary vane vacuum pump (Vacuubrand, Wertheim, Germany).

Analytical HPLC. Analytical HPLC analysis was performed with a system from Agilent Technologies composed of a 1290 Infinity binary pump equipped with a degasser, a 1290 Infinity autosampler, a 1290 Infinity thermostated column compartment, a 1260 Infinity diode array detector, and a 1260 Infinity fluorescence detector. A Kinetex-XB C18, 2.6 μm, 100 × 3 mm (Phenomenex) served as stationary phase at a flow rate of 0.6 mL/min. Detection was performed at 220 nm and the temperature of the column compartment was set to 25 °C. Mixtures of acetonitrile (A) and 0.04% aqueous TFA (B) were

https://doi.org/10.1021/acs.jmedchem.5c01701
J. Med. Chem. XXXX, XXX, XXX−XXX

used as mobile phase. The following linear gradients were applied: compounds **6** and **14**−**17b**: 0−14 min: A/B 10:90−30:70, 14−15 min: 30:70−95:5, 15−18 min: 95:5 (isocratic); compounds **10**, **24**, **26**, and **27**: 0−20 min: A/B 10:90−90:10, 20−21 min: 90:10−95:5, 21−25 min: 95:5 (isocratic); compounds **19** and **21**: 0−14 min: A/B 20:80−40:60, 14−15 min: 40:60−95:5, 15−18 min: 95:5 (isocratic). The injection volume was 20 μL. Retention (capacity) factors k were calculated from the retention times t_R according to $k = (t_R - t_0)/t_0$ (t_0 = dead time, 0.76 min for the used system and column).

General Procedure for Solid Phase Peptide Synthesis. Peptides were synthesized manually by SPPS on a 2-ClTrt resin according to the Fmoc strategy. 5 mL NORM-JECT syringes (B. Braun-Melsungen, Melsungen, Germany), equipped with a 35-μm polypropylene frit (Roland Vetter Laborbedarf, Ammerbuch, Germany), were used as reaction vessels. DMF/NMP 4:1 v/v was used as solvent for all amino acid coupling and Fmoc deprotection steps. Prior to the coupling of the first amino acid (**10**), the 2-ClTrt resin (loading: 1.60 mmol/g) was allowed to swell in CH_2Cl_2 for 30 min at rt followed by washing of the resin with CH_2Cl_2 (2×). Amino acid **10** was attached to the resin according to a reported procedure.[46] The loading of the resulting Fmoc-TMSAla-2-ClTrt resin, which was used for the synthesis of peptides **6** and **14**−**17b**, amounted to 1.00 mmol/g (determined photometrically *via* absorbance at 304 nm in DMF according to a reported protocol[47]). Fmoc deprotection of the Fmoc-TMSAla-2-ClTrt resin was carried out using 20% piperidine in DMF/NMP 4:1 v/v (2× 10 min at rt) followed by washing with solvent (6× ca. 1 mL). The following Fmoc-amino acids (except for **11**-**13**), used in 5-fold excess, were preactivated with HOBt/HBTU/DIPEA (5/4.9/10 equiv) in solvent (about 2.2 mL/mmol amino acid) for at least 5 min before addition to the resin. The Fmoc-protected unnatural amino acids **11**-**13** were used in 3-fold excess and were preactivated with HOBt/HBTU/DIPEA (3/3/6 equiv) in anhydrous solvent (about 1.6 mL/mmol amino acid) for 5−10 min prior to addition to the resin. Amino acid coupling was carried out on a shaker (Heidolph Multi Reax; Heidolph Instruments, Schwabach, Germany) covered with a thermostat controlled (35 °C) box. In the case of standard amino acids, "double" coupling (2× 45 min) was performed. **11**−**13** were attached by a single coupling procedure (35 °C, 16 h). After coupling of an Fmoc-amino acid, the resin was washed with solvent (4×) followed by Fmoc deprotection using 20% piperidine in solvent (2× 10 min at rt) and subsequent washing of the resin with solvent (6× ca. 1 mL). After coupling of the last amino acid and final Fmoc deprotection, the resin was washed with solvent (6×) and CH_2Cl_2 (3×) (treated with potassium carbonate). Peptides were cleaved off the resin using CH_2Cl_2/TFA 3:1 v/v (2× 20 min at rt). The liquids (2× ca. 2 mL) were collected in a 100 mL round-bottom flask and the resin was washed once with CH_2Cl_2/TFA 3:1 v/v (2 mL). The volatiles of the combined liquids were removed by evaporation, TFA/H_2O 95:5 v/v (2 mL per 100 mg resin) was added to the residue and the mixture was stirred at rt for 5 h. The volatiles were removed by evaporation followed by the addition of H_2O (ca. 50 mL) and lyophilization to obtain the crude peptide, which was subjected to purification by preparative HPLC.

Compound Characterization. Amino acid **7**, peptides **14**−**17b**, and compounds **24** and **26** were characterized by HRMS, ^{1}H-, ^{13}C-, and 2D-NMR spectroscopy (2D: ^{1}H-COSY, HSQC, HMBC), and RP-HPLC. Compounds **19** and **21** were characterized by HRMS, ^{1}H NMR spectroscopy, and RP-HPLC. **6** and **27** were characterized by HRMS and RP-HPLC. HPLC purities of all target compounds were ≥97% (UV detection, 220 nm).

Experimental Protocols and Analytical Data. *Lys-Lys-Pro-Tyr-Ile-β-trimethylsilyl-Ala Tris(hydrotrifluoroacetate) (**6**).*[19] Peptide **6** was synthesized on a Fmoc-TMSAla-2-ClTrt resin (50 mg, 1.00 mmol/g) according to the general procedure. Purification by preparative RP-HPLC (system 2, gradient: 0−30 min: acetonitrile/0.1% aqueous TFA 22:78−27:73, t_R = 7 min) yielded **6** as a white fluffy solid (29.4 mg, 52%). HRMS (ESI): m/z $[M+3H]^{3+}$ calcd. for $[C_{38}H_{69}N_8O_8Si]^{3+}$ 264.4997, found: 264.5001. RP-HPLC (220 nm): >99% (t_R = 8.6 min, k = 10.3). $C_{38}H_{66}N_8O_8Si \cdot C_6H_3F_9O_6$ (794.10 + 342.07).

*Arg-Arg-Pro-Tyr-Ile-β-trimethylsilyl-Ala Tris-(Hydrotrifluoroacetate) (**14**).* Peptide **14** was synthesized on a Fmoc-TMSAla-2-ClTrt resin (75 mg, 1.00 mmol/g) according to the general procedure. Purification by preparative RP-HPLC (system 1, gradient: 0−25 min: acetonitrile/0.1% aqueous TFA 15:85−45:55, t_R = 13 min) yielded **14** as a white fluffy solid (34.1 mg, 38%). ^{1}H NMR (600 MHz, DMSO-d_6): δ (ppm) 0.00 (s, 9H), 0.76−0.85 (m, 6H), 0.91−0.98 (m, 1H), 0.98−1.08 (m, 2H), 1.35−1.44 (m, 1H), 1.44−1.62 (m, 5H), 1.64−1.76 (m, 4H), 1.77−1.90 (m, 3H), 1.93−2.03 (m, 1H), 2.62−2.70 (m, 1H), 2.80−2.93 (m, 1H), 3.03−3.12 (m, 4H), 3.54−3.61 (m, 2H, interfering with the water signal, quantified in the spectrum acquired after the addition of D_2O), 3.81−3.84 (m, 1H, interfering with the water signal, quantified in the spectrum acquired after the addition of D_2O), 4.18−4.26 (m, 2H), 4.31−4.36 (m, 1H), 4.37−4.43 (m, 1H), 4.44−4.53 (m, 1H), 6.59−6.64 (m, 2H), 6.84−7.28 (br s, 4H, interfering with next listed signal), 6.99−7.03 (m, 2H), 7.28−7.65 (br s, 4H), 7.73 (d, 1H, J 9.2 Hz), 7.81 (t, 1H, 5.5 Hz), 7.86 (t, 1H, J 6.2 Hz), 7.94 (d, 1H, J 8.1 Hz), 8.13−8.29 (m, 4H), 8.67 (d, 1H, J 7.3 Hz), 9.23 (s, 1H), 12.45 (s, 1H). ^{13}C NMR (150 MHz, DMSO-d_6): δ (ppm) 0.00 (3 carbon atoms), 10.89, 15.13, 19.28, 24.03, 24.09, 24.17, 24.61, 28.21, 28.42, 29.10, 36.43, 37.27, 40.16, 40.53, 46.85, 48.63, 50.46, 51.69, 54.28, 56.32, 59.15, 113.96 (TFA), 114.85 (2 carbon atoms), 115.93 (TFA), 117.90 (TFA), 119.88 (TFA), 127.80, 130.11 (2 carbon atoms), 155.79, 156.92, 156.94, 158.88 (q, J 32 Hz) (TFA), 168.31, 169.24, 170.54, 170.75, 171.37, 174.61. HRMS (ESI): m/z $[M + 3H]^{3+}$ calcd for $[C_{38}H_{69}N_{12}O_8Si]^{3+}$ 283.1705, found: 283.1716. RP-HPLC (220 nm): >99% (t_R = 9.0 min, k = 10.8). $C_{38}H_{66}N_{12}O_8Si \cdot C_6H_3F_9O_6$ (847.11 + 342.07).

*N^{α}-Methyl-Arg-Arg-Pro-Tyr-Ile-β-trimethylsilyl-Ala Tris-(hydrotrifluoroacetate) (**15**).* Peptide **15** was synthesized on a Fmoc-TMSAla-2-ClTrt resin (75 mg, 1.00 mmol/g) according to the general procedure. Purification by preparative HPLC (system 1, gradient: 0−25 min: acetonitrile/0.1% aqueous TFA 15:85−45:55, t_R = 14 min) yielded **15** as a white fluffy solid (40.3 mg, 44%).^{1}H NMR (600 MHz, DMSO-d_6): δ (ppm) 0.00 (s, 9H), 0.76−0.86 (m, 6H), 0.91−0.98 (m, 1H), 0.98−1.07 (m, 2H), 1.38−1.48 (m, 3H), 1.51−1.59 (m, 3H), 1.66−1.76 (m, 4H), 1.79−1.87 (m, 3H), 1.94−2.04 (m, 1H), 2.46−2.48 (m, 3H), 2.62−2.69 (m, 1H), 2.82−2.88 (m, 1H), 3.06−3.15 (m, 4H), 3.55−3.60 (m, 2H, interfering with the water signal, quantified in the spectrum acquired after the addition of D_2O), 3.78−3.81 (m, 1H, interfering with the water signal, quantified in the spectrum acquired after the

https://doi.org/10.1021/acs.jmedchem.5c01701
J. Med. Chem. XXXX, XXX, XXX−XXX

addition of D_2O), 4.17−4.28 (m, 2H), 4.32−4.36 (m, 1H), 4.38−4.43 (m, 1H), 4.52−4.57 (m, 1H), 6.60−6.63 (m, 2H), 6.82−7.29 (br s, 4H, interfering with next listed signal), 7.00−7.02 (m, 2H), 7.29−7.65 (br s, 4H), 7.71−7.75 (m, 1H), 7.84−7.90 (m, 2H), 7.93 (d, 1H, *J* 8.1 Hz), 8.20 (d, 1H, *J* 7.9 Hz), 8.87 (d, 1H, *J* 7.3 Hz), 8.95 (s, 1H), 9.04−9.70 (m, 2H), 12.46 (s, 1H). ^{13}C NMR (150 MHz, DMSO-d_6): δ (ppm) 0.00 (3 carbon atoms), 10.89, 15.13, 19.28, 23.92, 24.03, 24.18, 24.62, 26.99, 28.12, 29.09, 31.16, 36.42, 37.27, 40.08, 40.44, 46.86, 48.63, 50.58, 54.27, 56.32, 59.16, 59.92, 113.94 (TFA), 114.85 (2 carbon atoms), 115.91 (TFA), 117.88 (TFA), 119.86 (TFA), 127.80, 130.11 (2 carbon atoms), 155.78, 156.93 (2 carbon atoms), 158.91 (q, *J* 33 Hz) (TFA), 167.00, 169.06, 170.54, 170.74, 171.33, 174.60. HRMS (ESI): *m*/*z* [M + 3H]$^{3+}$ calcd for $[C_{39}H_{71}N_{12}O_8Si]^{3+}$ 287.8424, found: 287.8434. RP-HPLC (220 nm): >99% (t_R = 9.2 min, *k* = 11.1). $C_{39}H_{68}N_{12}O_8Si{\cdot}C_6H_3F_9O_6$ (861.13 + 342.07).

*N$^{\alpha}$-Methyl-Arg-Arg-Pro-β,β-dimethyl-L-Tyr-Ile-β-trimethylsilyl-Ala Tris(hydrotrifluoroacetate) (**16a**) and N$^{\alpha}$-Methyl-Arg-Arg-Pro-β,β-dimethyl-D-Tyr-Ile-β-trimethylsilyl-Ala Tris(hydrotrifluoroacetate) (**16b**).* Peptides **16a** and **16b**, representing diastereomers, were synthesized on a Fmoc-TMSAla-2-ClTrt resin (50 mg, 1.00 mmol/g) according to the general procedure. The unavailability of enantiomerically pure Fmoc-β,β-dimethyl-L-Tyr(*t*Bu)−OH (this Fmoc amino acid was only available as racemic mixture) necessitated the synthesis of both diastereomers, which were separated by preparative HPLC (system 1, gradient: 0−25 min: acetonitrile/0.1% aqueous TFA 15:85−45:55, t_R (**16a**) = 14 min, t_R (**16b**) = 16 min). Lyophilization of the eluates yielded **16a** and **16b** as white fluffy solids (**16a**: 23.0 mg, 37%; **16b**: 21.1 mg, 34%). ^{1}H NMR of **16a** (600 MHz, DMSO-d_6): δ (ppm) 0.00 (s, 9H), 0.73−0.85 (m, 6H), 0.90−1.04 (m, 3H), 1.19−1.30 (m, 6H), 1.33−1.42 (m, 1H), 1.42−1.50 (m, 2H), 1.50−1.61 (m, 3H), 1.61−1.84 (m, 7H), 1.84−1.95 (m, 1H), 2.48 (s, 3H), 3.04−3.17 (m, 4H), 3.48−3.53 (m, 1H, interfering with the water signal, quantified in the spectrum acquired after the addition of D_2O), 3.55−3.59 (m, 1H, interfering with the water signal, quantified in the spectrum acquired after the addition of D_2O), 3.82 (s, 1H, interfering with the water signal, quantified in the spectrum acquired after the addition of D_2O), 4.14 (t, 1H, *J* 8.4 Hz), 4.14−4.24 (m, 1H), 4.36−4.43 (m, 1H), 4.52−4.58 (m, 1H), 4.60−4.69 (m, 1H), 6.59−6.65 (m, 2H), 6.93−7.30 (br s, 4H, interfering with next listed signal), 7.11−7.14 (m, 2H), 7.30−7.81 (m, 6H), 7.84−7.94 (m, 2H), 8.08 (d, 1H, *J* 7.8 Hz), 8.92 (d, 1H, *J* 8.0 Hz), 8.95 (s, 1H), 9.04−9.41 (m, 2H), 12.42 (s, 1H). ^{13}C NMR of **16a** (150 MHz, DMSO-d_6): δ (ppm) 0.00 (3 carbon atoms), 10.94, 15.13, 19.22, 23.92, 24.11, 24.14, 24.45, 24.55, 26.99, 27.09, 28.13, 28.63, 31.16, 37.08, 40.06, 40.16, 40.43, 46.86, 48.68, 50.51, 56.43, 59.25, 59.88, 59.91, 114.07 (TFA), 114.34 (2 carbon atoms), 116.05 (TFA), 118.02 (TFA), 120.00 (TFA), 127.42 (2 carbon atoms), 136.42, 155.26, 156.90, 156.95, 158.83 (q, *J* 32 Hz) (TFA), 167.05, 169.35, 169.42, 170.43, 170.56, 174.66. ^{1}H NMR of **16b** (600 MHz, DMSO-d_6): δ (ppm) 0.00 (s, 9H), 0.71−0.82 (m, 6H), 0.88−1.03 (m, 3H), 1.17−1.34 (m, 8H), 1.40−1.49 (m, 2H), 1.49−1.64 (m, 5H), 1.64−1.85 (m, 5H), 2.47 (s, 3H), 3.01−3.17 (m, 4H), 3.41−3.50 (m, 1H, interfering with the water signal, quantified in the spectrum acquired after the addition of D_2O), 3.51−3.58 (m, 1H, interfering with the water signal, quantified in the spectrum acquired after the addition of D_2O), 3.80 (s, 1H, interfering with the water signal, quantified in the spectrum acquired after the addition of D_2O), 4.10 (q, 1H, *J* 7.3 Hz), 4.13−4.19 (m, 1H), 4.35−4.42 (m, 1H), 4.47−4.54 (m, 1H), 4.87 (d, 1H, *J* 9.9 Hz), 6.57−6.67 (m, 2H), 6.74−7.26 (br s, 4H, interfering with next listed signal), 7.14−7.17 (m, 2H), 7.26−7.59 (br s, 4H), 7.62 (d, 1H, *J* 8.5 Hz), 7.69 (d, 1H, *J* 9.8 Hz), 7.79−7.90 (m, 2H), 8.19 (d, 1H, *J* 7.0 Hz), 8.85 (d, 1H, *J* 7.1 Hz), 8.94 (s, 1H), 9.00−9.56 (m, 2H), 12.43 (s, 1H). ^{13}C NMR of **16b** (150 MHz, DMSO-d_6): δ (ppm) 0.00 (3 carbon atoms), 11.09, 15.26, 19.25, 23.84, 23.99, 24.01, 24.15, 24.55, 26.53, 26.97, 28.02, 29.40, 31.14, 37.09, 40.09, 40.43, 41.00, 46.71, 49.31, 50.60, 56.41, 59.15, 59.49, 59.86, 114.06 (TFA), 114.35 (2 carbon atoms), 116.03 (TFA), 118.02 (TFA), 120.00 (TFA), 127.29 (2 carbon atoms), 136.86, 155.38, 156.92 (2 carbon atoms), 158.74 (q, *J* 32 Hz) (TFA), 166.95, 168.97, 169.40, 170.17, 170.84, 174.48. HRMS (ESI): *m*/*z* [M + 3H]$^{3+}$ calcd for $[C_{41}H_{75}N_{12}O_8Si]^{3+}$ 297.1861, found: 297.1866 (**16a**), 297.1866 (**16b**). RP-HPLC (220 nm): **16a**: 99% (t_R = 10.7 min, *k* = 13.1), **16b**: 97% (t_R = 12.2 min, *k* = 15.1). $C_{41}H_{72}N_{12}O_8Si{\cdot}C_6H_3F_9O_6$ (889.19 + 342.07).

*N$^{\alpha}$-Methyl-N$^{\omega}$-[(4-aminobutyl)aminocarbonyl]Arg-Arg-Pro-β,β-dimethyl-L-Tyr-Ile-β-trimethylsilyl-Ala Tetrakis(hydrotrifluoroacetate) (**17a**) and N$^{\alpha}$-Methyl-N$^{\omega}$-[(4-aminobutyl)aminocarbonyl]Arg-Arg-Pro-β,β-dimethyl-D-Tyr-Ile-β-trimethylsilyl-Ala Tetrakis(hydrotrifluoroacetate) (**17b**).* Peptides **17a** and **17b**, representing diastereomers, were synthesized on a Fmoc-TMSAla-2-ClTrt resin (150 mg, 1.00 mmol/g) according to the general procedure with the following modification: after coupling of the last amino acid and Fmoc-deprotection, the resin was washed with CH_2Cl_2 (5×), a solution of 2-nitrobenzenesulfonyl chloride (100 mg, 0.45 mmol) and collidine (100 μL, 0.75 mmol) in CH_2Cl_2 (3.5 mL) was added and the mixture was shaken at rt for 2 h. The resin was washed with DMF (5×) and a solution of MTBD (87 μL, 0.6 mmol) and methyl-4-nitrobenzenesulfonate (163 mg, 0.75 mmol) in DMF (4.2 mL) was added followed by shaking at rt for 30 min. After washing the resin with DMF (3×), a solution of DBU (112 μL, 0.75 mmol) and 2-mercaptoethanol (104 μL, 1.5 mmol) in DMF (3.5 mL) was added and the mixture was shaken at rt for 30 min. The resin was washed with DMF (5×) followed by cleavage from the resin as described in the general procedure for SPPS. The unavailability of enantiomerically pure Fmoc-β,β-dimethyl-L-Tyr(*t*Bu)−OH (only available as racemic mixture) necessitated the synthesis of both diastereomers, which were separated by preparative RP-HPLC (system 1, gradient: 0−25 min: acetonitrile/0.1% aqueous TFA 15:85−45:55, t_R (**17a**) = 12 min, t_R (**17b**) = 14 min). Lyophilization of the eluates yielded **17a** and **17b** as white fluffy solids (**17a**: 30.1 mg, 14%; **17b**: 27.8 mg, 13%). ^{1}H NMR of **17a** (600 MHz, DMSO-d_6): δ (ppm) 0.00 (s, 9H), 0.72−0.89 (m, 6H), 0.90−1.04 (m, 3H), 1.18−1.31 (m, 6H), 1.33−1.42 (m, 1H), 1.43−1.61 (m, 9H), 1.62−1.94 (m, 8H), 2.47 (s, 3H), 2.73−2.83 (m, 2H), 3.03−3.18 (m, 4H), 3.21−3.30 (m, 2H), 3.46−3.54 (m, 1H), 3.54−3.63 (m, 1H), 3.76−3.91 (m, 1H), 4.12 (t, 1H, *J* 7.1 Hz), 4.16−4.25 (m, 1H), 4.36−4.43 (m, 1H), 4.48−4.59 (m, 1H), 4.66 (d, 1H, *J* 9.6 Hz), 6.57−6.65 (m, 2H), 6.71−7.28 (br s, 2H, interfering with next listed signal), 7.11−7.14 (m, 2H), 7.28−7.70 (m, 5H), 7.71−7.99 (m, 4H), 8.06 (d, 1H, *J* 7.9 Hz), 8.52 (s, 2H), 8.68−9.15 (m, 3H), 9.17 (s, 1H), 10.78 (s, 1H), 12.41 (s, 1H). One exchangeable proton (NH) of the presumably 4-fold protonated molecule could not be identified. ^{13}C NMR of **17a** (150 MHz, DMSO-d_6): δ (ppm) 0.00 (3 carbon atoms), 10.95, 15.14, 19.25, 23.43,

https://doi.org/10.1021/acs.jmedchem.5c01701
J. Med. Chem. XXXX, XXX, XXX−XXX

24.11, 24.16, 24.38, 24.54 (2 carbon atoms), 25.99, 27.00 (2 carbon atoms), 28.16, 28.64, 32.16, 37.08, 38.49, 38.64, 40.06, 40.14, 40.43, 46.86, 48.71, 50.50, 56.45, 59.25, 59.88 (2 carbon atoms), 114.12 (TFA), 114.35 (2 carbon atoms), 116.10 (TFA), 118.08 (TFA), 120.06 (TFA), 127.42 (2 carbon atoms), 136.40, 153.93 (2 carbon atoms), 155.27, 156.94, 158.90 (q, *J* 32 Hz) (TFA), 167.14, 169.32, 169.39, 170.42, 170.58, 174.69. ^{1}H NMR of **17b** (600 MHz, DMSO-d_6): δ (ppm) 0.00 (s, 9H), 0.70−0.82 (m, 6H), 0.87−1.02 (m, 3H), 1.19−1.35 (m, 8H), 1.44−1.65 (m, 11H), 1.65−1.83 (m, 5H), 2.47 (s, 3H), 2.75−2.83 (m, 2H), 3.04−3.16 (m, 4H), 3.21−3.30 (m, 2H), 3.43−3.50 (m, 1H), 3.50−3.58 (m, 1H), 3.81 (s, 1H), 4.11 (q, 1H, *J* 7.6 Hz), 4.15 (t, 1H, *J* 7.4 Hz), 4.36−4.41 (m, 1H), 4.49−4.55 (m, 1H), 4.86 (d, 1H, *J* 9.8 Hz), 6.57−6.65 (m, 2H), 6.73−7.32 (br s, 2H, interfering with next listed signal), 7.14−7.17 (m, 2H), 7.32−7.72 (m, 5H), 7.72−8.04 (m, 4H), 8.17 (d, 1H, *J* 7.0 Hz), 8.53 (s, 2H), 8.87 (d, 1H, *J* 7.3 Hz), 8.96 (s, 1H), 9.05−9.23 (m, 2H), 10.88 (s, 1H), 12.43 (s, 1H). One exchangeable proton (NH) of the presumably 4-fold protonated molecule could not be identified. ^{13}C NMR of **17b** (150 MHz, DMSO-d_6): δ (ppm) 0.00 (3 carbon atoms), 11.09, 15.26, 19.26, 23.37, 23.99, 24.02, 24.20, 24.39, 24.55, 25.99, 26.48, 26.91, 28.10, 29.32, 31.14, 37.10, 38.49, 38.66, 40.11, 40.44, 40.98, 46.71, 49.26, 50.59, 56.39, 59.17, 59.55, 59.81, 114.07 (TFA), 114.37 (2 carbon atoms), 116.04 (TFA), 118.01 (TFA), 119.98 (TFA), 127.29 (2 carbon atoms), 136.86, 153.94 (2 carbon atoms), 155.40, 156.97, 158.97 (q, *J* 32 Hz) (TFA), 166.92, 168.99, 169.34, 170.19, 170.81, 174.50. HRMS (ESI): *m*/*z* [M + 3H]$^{3+}$ calcd. for $[C_{46}H_{85}N_{14}O_9Si]^{3+}$ 335.2126, found: 335.2135 (**17a**), 335.2132 (**17b**). RP-HPLC (220 nm): **17a**: 97% (t_R = 9.5 min, k = 11.5), **17b**: 99% (t_R = 10.9 min, k = 13.3). $C_{46}H_{82}N_{14}O_9Si{\cdot}C_8H_4F_{12}O_8$ (1003.34 + 456.09).

*N$^{\alpha}$-Methyl-N$^{\omega}$-{[4-(N-{1-carboxylato[2-(6-(dimethylamino)-3-(dimethyliminio))-3H-xanthen-9-yl]phen-5-yl}-carbonyl)-aminobutyl]aminocarbonyl}Arg-Arg-Pro-β,β-dimethyl-L-Tyr-Ile-β-trimethylsilyl-Ala Tris(hydro-trifluoroacetate) (**19**).* Peptide **17a** (3.4 mg, 2.3 μmol) and DIPEA (4.7 μL, 27 μmol) were dissolved in DMF/NMP 8:2 v/v (100 μL) followed by the addition of a solution of 5-TAMRA succinimidyl ester **18** (1.1 mg, 2.1 μmol) in DMF/NMP 8:2 v/v (30 μL). After stirring at room temperature in the dark for 1 h, the mixture was diluted with 10% aqueous TFA (14 μL) and acetonitrile/0.1% aqueous TFA 20:80 v/v (1 mL). Isolation by preparative RP-HPLC (system 1, gradient: 0−35 min: acetonitrile/0.1% aqueous TFA 20:80−60:40, t_R = 16 min) gave **19** as a purple fluffy solid (1.6 mg, 40%) ^{1}H NMR (600 MHz, DMSO-d_6): δ (ppm) 0.00 (s, 9H), 0.73−0.83 (m, 6H), 0.92−1.03 (m, 3H), 1.22−1.29 (m, 6H), 1.34−1.41 (m, 1H), 1.49−1.61 (m, 9H), 1.62−1.68 (m, 1H), 1.68−1.86 (m, 6H), 1.86−1.96 (m, 1H), 2.45−2.48 (m, 3H), 3.07−3.18 (m, 6H), 3.27 (s, 12H), 3.33−3.36 (m, 2H, interfering with the water signal, quantified in the spectrum acquired after the addition of D_2O), 3.51−3.52 (m, 1H, interfering with the water signal, quantified in the spectrum acquired after the addition of D_2O), 3.58−3.59 (m, 1H, interfering with the water signal, quantified in the spectrum acquired after the addition of D_2O), 3.81−3.84 (m, 1H, interfering with the water signal, quantified in the spectrum acquired after the addition of D_2O), 4.13 (t, 1H, *J* 7.8 Hz), 4.18−4.23 (m, 1H), 4.39−4.44 (m, 1H), 4.54−4.60 (m, 1H), 4.66 (d, 1H, *J* 9.1 Hz), 6.31−6.72 (br s, 1H, interfering with next listed signal), 6.59−6.64 (m, 2H), 6.82−7.17 (m, 9H), 7.18−7.48 (br s, 2H, interfering with next listed signal), 7.39 (d, 1H, *J* 9.3 Hz), 7.48−7.62 (m, 3H), 7.68 (t, 1H, *J* 5.1 Hz), 8.08 (d, 1H, *J* 7.6 Hz), 8.28 (d, 1H, *J* 7.6 Hz), 8.47 (s, 2H), 8.61−8.74 (m, 1H), 8.81−9.24 (m, 6H), 10.30 (s, 1H), 12.40 (s, 1H), 13.40 (s, 1H). HRMS (ESI): *m*/*z* [M + 3H]$^{3+}$ calcd. for $[C_{71}H_{105}N_{16}O_{13}Si]^{3+}$ 472.5933, found: 472.5942. RP-HPLC (220 nm): 99% (t_R = 8.8 min, k = 10.6). $C_{71}H_{102}N_{16}O_{13}Si{\cdot}C_6H_3F_9O_6$ (1415.78 + 342.07).

*N$^{\alpha}$-Methyl-N$^{\omega}$-{[4-(N-{6-3H-[2-(5−3H-(1-(4-sulfonatobutyl)-3,3-dimethyl)indol-2-ylidenepent-1,3-dienyl)-3,3-dimethyl-5-sulfo]indol-1-ium-1-yl}hexanoyl)-aminobutyl]-aminocarbonyl}Arg-Arg-Pro-β,β-dimethyl-L-Tyr-Ile-β-trimethylsilyl-Ala Tris(hydrotrifluoroacetate) (**21**).* Peptide **17a** (3.3 mg, 2.3 μmol) and DIPEA (4.6 μL, 26 μmol) were dissolved in DMF/NMP 8:2 v/v (100 μL) followed by the addition of the sulfo-Cy5 succinimidyl ester **20** (1.1 mg, 2.1 μmol) in DMF/NMP 8:2 v/v (30 μL). After stirring at room temperature in the dark for 1 h, the mixture was diluted with 10% aqueous TFA (14 μL) and 0.1% acetonitrile/aqueous TFA 20:80 v/v (1 mL). Isolation by preparative RP-HPLC (system 1, gradient: 0−35 min: acetonitrile/0.1% aqueous TFA 20:80−60:40, t_R = 17 min) gave **21** as a purple fluffy solid (1.4 mg, 30%). ^{1}H NMR (600 MHz, DMSO-d_6): δ (ppm) 0.00 (s, 9H), 0.73−0.83 (m, 6H), 0.91−1.01 (m, 3H), 1.21−1.29 (m, 6H), 1.28−1.44 (m, 8H), 1.48−1.59 (m, 7H), 1.63−1.71 (m, 15H), 1.71−1.84 (m, 9H), 1.85−1.95 (m, 1H), 2.04 (t, 2H, *J* 6.4 Hz), 2.46−2.48 (m, 3H), 2.64 (t, 2H, *J* 6.8 Hz), 2.98−3.03 (m, 2H), 3.06−3.14 (m, 4H, interfering with the water signal, quantified in the spectrum acquired after the addition of D_2O), 3.22−3.26 (m, 2H, interfering with the water signal, quantified in the spectrum acquired after the addition of D_2O), 3.55−3.57 (m, 2H, interfering with the water signal, quantified in the spectrum acquired after the addition of D_2O), 3.80−3.84 (m, 1H, interfering with the water signal, quantified in the spectrum acquired after the addition of D_2O), 4.03−4.09 (m, 2H), 4.10−4.16 (m, 3H), 4.17−4.23 (m, 1H), 4.39−4.44 (m, 1H), 4.52−4.58 (m, 1H), 4.64 (d, 1H, *J* 9.3 Hz), 6.24 (d, 1H, *J* 13.7 Hz), 6.39 (d, 1H, *J* 14.0 Hz), 6.53−6.65 (m, 3H), 6.68−7.06 (br s, 2H), 7.09−7.16 (m, 2H), 7.20−7.32 (m, 3H), 7.32−7.58 (m, 7H), 7.61−7.67 (m, 2H), 7.78 (t, 1H, *J* 5.5 Hz), 7.81−7.84 (m, 1H), 8.08 (d, 1H, *J* 7.7 Hz), 8.25−8.48 (m, 4H), 8.74−9.05 (m, 4H), 9.06−9.18 (m, 1H), 9.99 (s, 1H), 12.40 (s, 1H). HRMS (ESI): *m*/*z* [M + 3H]$^{3+}$ calcd. for $[C_{81}H_{126}N_{16}O_{16}S_2Si]^{3+}$ 557.2937, found: 557.2943. RP-HPLC (220 nm): 99% (t_R = 10.1 min, k = 12.3). $C_{81}H_{123}N_{16}O_{16}S_2Si{\cdot}C_6H_3F_9O_6$ (1669.18 + 342.07).

Capillary Electrophoresis. Capillary electrophoresis was performed with an Agilent 7100 CE system using a bare fused silica capillary with an inner diameter of 0.05 mm and a length of 72 cm (G1600−62211, Agilent). 50 mM α-cyclodextrin (Honeywell, Charlotte, United States) in a 125 mM sodium phosphate buffer (pH = 7.0) served as electrolyte solution. Injections were performed hydrodynamically applying a pressure of 100 mbar for 10 s. The temperature of the capillary housing was set to 30 °C. A voltage of 20 kV was applied for 35 min and the detection was performed at 220 nm.

Chemical Stability. The chemical stability of peptides **19** and **21** was investigated in PBS (adjusted to pH = 7.4) at 22 °C in the dark. The incubation was started by the addition of 3 μL of a 5 mM stock solution (solvent: DMSO) to 147 μL of PBS to yield a concentration of 100 μM. After periods of 0, 6, 24, and 48 h, an aliquot (25 μL) was removed and added to 25 μL of acetonitrile/0.04% aq. TFA 2:8 v/v to obtain a peptide

https://doi.org/10.1021/acs.jmedchem.5c01701
J. Med. Chem. XXXX, XXX, XXX−XXX

solution with a concentration of 50 μM. 20 μL of this solution were subjected to analytical RP-HPLC analysis using the same system and conditions as described under *Analytical HPLC*. A 1:1 mixture of PBS and acetonitrile/0.04% aq. TFA 2:8 v/v (20 μL) was analyzed to obtain the blank chromatogram.

Stability in Human Plasma. The proteolytic stabilities of NT(8−13), **15**, **17a**, **19** and **21** were investigated in human blood plasma/PBS 1:2 v/v according to a described procedure.[16] Samples were analyzed using the RP-HPLC system and conditions as described under *Analytical HPLC* with the following gradient: 0−6 min: acetonitrile/0.04% aq. TFA 10:90−21:79, 6−12 min: 21:79−40:60, 12−13 min: 40:60−95:5, 13−16 min: 95:5 (isocratic). Data analysis was based on UV detection at 220 nm. Reference samples, representing 100% recovery, were prepared in quadruplicate. Recovery ratios were obtained by dividing the recovery of the peptide by the recovery of IS for each individual sample (n = 3−5). The obtained recoveries and the recovery ratios are summarized in Table S1.

Excitation Spectra, Emission Spectra, and Fluorescence Quantum Yields. Absorption spectra were recorded with a referenced single beam spectrometer (Cary 60, Agilent) and the emission and excitation spectra were recorded in an orthogonal configuration in an emission spectrometer (Fluorolog, Horiba) setting the resolution to 1 nm for excitation and emission detection. The fluorescence decays were recorded with a self-constructed Time Correlated Single Photon Counting (TCSPC) setup[48] with single detection wavelength at room temperature. The sample was excited along a 10 mm path length at λ_{ex} = 280 nm and the emission was recorded orthogonally to this along a 2 mm path length at λ_{obs} as indicated in Figure S7. The optical density of the sample was set to ca. 0.1 at the excitation wavelength over 10 mm path length. The fluorescence quantum yields of compounds **19** and **21** were determined in PBS and PBS supplemented with 1% BSA *via* an absolute method using an Ulbricht sphere with an inaccuracy of ca. 3% (Hamamatsu C9920−02 system equipped with a Spectralon integrating sphere) at room temperature using a 10 mm × 10 mm quartz cuvette. The optical density at the excitation wavelength of the sample was <0.1 along an optical path length of 1 cm.

Cell Culture. Mammalian cells were cultured in T75 or T175 culture flasks (Sarstedt). Chinese hamster ovary (CHO) cells stably expressing hNTS$_1$R[28] were cultured in DMEM/HAM's F12 (Sigma, Taufkirchen, Germany) medium (1:1) supplemented with 7.5% FBS, L-glutamine (Sigma) (630 μg/mL), and hygromycin B (Carl Roth, Karlsruhe, Germany) (250 μg/mL). HT-29 colon carcinoma cells (DSMZ-no. ACC 299) were grown in antibiotic-free RPMI-164 medium (Sigma) supplemented with 7.5% FBS or in MEM Earles medium supplemented with 10% FBS, 1% L-glutamine, 1% NEAA, and 1% pyruvate. HEK293T-hNTS$_2$R cells were cultured in Dulbecco's modified Eagle's medium (Sigma-Aldrich) supplemented with 10% FBS, L-glutamine (2 mM) and penicillin−streptomycin (100 IU/mL and 0.1 mg/mL, respectively) (Sigma-Aldrich). All cell lines were cultured in a humidified atmosphere (95% air and 5% CO_2) at 37 °C.

Buffers Used for Binding and Functional Assays. *DPBS*: Dulbecco's phosphate-buffered saline with calcium and magnesium (1.8 mM $CaCl_2$, 2.68 mM KCl, 1.47 mM KH_2PO_4, 3.98 mM $MgSO_4$, 137 mM NaCl, 8.06 mM Na_2HPO_4, pH = 7.4) supplemented with 0.1% BSA (flow cytometry) or 1% BSA (radiochemical assays) and 0.1 mg/mL bacitracin. For flow cytometric binding studies, *DPBS* was filtrated using 0.2 μm nylon syringe filters (Phenomenex).

Fura-2 assay buffer: HEPES buffer (120 mM NaCl, 5 mM KCl, 2 mM $MgCl_2$, 1.5 mM $CaCl_2$, 25 mM HEPES, and 10 mM glucose at pH = 7.4) supplemented with 2% BSA and 2.5 mM Probenecid (Sigma).

Radiochemical Competition Binding Assays with [^{3}H]UR-MK300. NTS$_1$R radioligand competition binding experiments with [^{3}H]UR-MK300 (molar activity: 2.41 TBq/mmol) and the peptides under study were performed with intact hNTS$_1$R-expressing human HT-29 colon carcinoma cells at 23 ± 1 °C using a previously reported protocol.[12] The K_d value of the radioligand for the used batch of [^{3}H]UR-MK300 was determined recently (K_d = 0.41 nM).[21] Cells were seeded 1 day before the assay, yielding a confluency of at least 90% on the day of the experiment. Total binding data (including total binding in the absence of competitor) were plotted as dpm values against log(concentration competitor) and analyzed by a four-parameter logistic equation (log(inhibitor) vs response − variable slope, GraphPad Prism 5, GraphPad Software, San Diego, CA) to obtain pIC_{50} values. Individual pIC_{50} values were converted to pK_i values according to the Cheng-Prusoff equation[49] (logarithmic form). To plot average data from individual binding experiments, data were normalized (100% = "top" of the four-parameter logistic fit, 0% = nonspecifically bound radioligand).

NTS$_2$R radioligand competition binding experiments with [^{3}H]UR-MK300 were performed with membranes of HEK293T-hNTS$_2$R.[21] Membrane preparations were prepared using a recently reported protocol for membrane preparations of CHO-hNTS$_1$R cells.[16] The protein concentration amounted to 1.8 ± 0.2 mg/mL (mean value ± SEM from three different sample dilutions). NTS$_2$R saturation and competition binding experiments with [^{3}H]UR-MK300 were carried out as described for saturation and competition binding studies with [^{3}H]UR-FE051 at membrane preparations of CHO-hNTS$_1$R cells.[16] The soluble protein concentration in the assays was 135 μg/mL. The K_d value of [^{3}H]UR-MK300 amounted to 3.1 ± 0.2 nM (mean value ± SEM from three independent experiments, each performed in triplicate). The concentration of [^{3}H]UR-MK300 in the competition binding assays was 5 nM. Data from competition binding assays were processed as the data from the NTS$_1$R binding assays.

Fura-2 Ca^{2+} Assay. The Fura-2 Ca^{2+} assay was conducted as previously described[16] with the following modifications: HT-29 cells were used in place of CHO-hNTS$_1$R cells and 1 μM NT(8−13) was used to determine the maximal response. Measurements were performed in black 96-well plates (Greiner 655076, Greiner Bio-One, Frickenhausen, Germany) and a measurement for one well comprised 40 cycles (instead of 44 cycles) with a cycle duration of 1.4 s (total time: 56 s).

Flow Cytometric Binding Experiments. Flow cytometry-based NTS$_1$R binding studies were performed with intact HT-29 (all kind of experiments) and CHO-hNTS$_1$R cells (only saturation binding) using a BD FACSCanto II flow cytometer (Becton Dickinson, Heidelberg, Germany), equipped with an argon laser (488 nm), a red diode laser (640 nm), and a BD High Throughput Sampler (HTS unit) for microtiter plates. Saturation and competition binding experiments were performed in triplicate in 96-well polypropylene plates (Brand 701330, Wertheim, Germany) using the HTS unit for sample injection. Association and dissociation experiments were performed in triplicate in 5 mL polypropylene tubes (VWR,

https://doi.org/10.1021/acs.jmedchem.5c01701
J. Med. Chem. XXXX, XXX, XXX−XXX

Radnor, USA), from which samples were directly injected into the flow cytometer. The following gain settings for forward and sideward scatter were applied: FSC, 0 V; SSC, 252 V. Fluorescence was recorded using the PE channel (excitation: 488 nm, emission: 585 ± 21 nm) with a PMT gain of 400−500 V (**19**) or the APC channel (excitation: 640 nm, emission: 660 ± 10 nm) with a PMT gain of 380−580 V (**21**). For measurements using the HTS unit, 45 μL of the sample were injected with a speed of 1.5 μL/s. For measurements, using an injection from 5 mL sample tubes, the medium flow rate (60 μL/min) was used. Measurements were stopped after 30 s (HTS unit) or after counting of at least 3000 gated events (injection from sample tubes).

Cells were seeded in T75 culture flasks 3−4 days (CHO-hNTS$_1$R cells) or 5−6 days (HT-29 cells) prior to the experiment. On the day of the experiment, cells were detached by trypsinization, suspended in *DPBS* and centrifuged at 200 g at rt for 5 min. The cell pellet was resuspended in binding buffer and the cell density was adjusted to 1.5×10^4 or 1.5×10^5 cells/mL (CHO-hNTS1R cells) or 5.0×10^5 cells/mL (HT-29 cells). Nonspecific binding was determined in the presence of 1 μM NT(8−13).

Saturation Binding Experiments. A 96-well polypropylene plate was prefilled with 200 μL of cell suspension. For total binding, H_2O (2 μL) and DMSO/H_2O 2:8 v/v (2 μL) containing the fluorescent ligand (100-fold concentrated compared to the final concentration) were added. To determine nonspecific binding, a 100 μM solution of NT(8−13) in H_2O (2 μL) and DMSO/H_2O 2:8 v/v (2 μL) containing the fluorescent ligand (100-fold concentrated) were added. Samples were incubated at 23 ± 1 °C in the dark under gentle shaking for 2 h followed by measurement *via* the HTS unit. Specific binding data, obtained by subtracting triplicate mean values of nonspecific binding from triplicate mean values of total binding, were plotted against the fluorescent ligand concentration and analyzed by a two-parameter equation describing hyperbolic single-site binding (one site, specific binding, GraphPad Prism 5) to obtain K_d values.

Association Experiments. 5 mL polypropylene tubes were prefilled with 2000 μL of cell suspension and H_2O (20 μL) was added (determination of total binding). To start the association, a 100-fold concentrated solution (compared to the final concentration) of the fluorescent ligand in DMSO/H_2O 2:8 v/v (20 μL) was added (final concentrations: **19**: 1 nM, **21**: 0.1 nM). The sample tubes were gently shaken in the dark at 23 ± 1 °C. Measurements were conducted within different periods of time (1−240 min) by placing the tubes in the injection port of the cytometer. To determine nonspecific binding, samples were set up as in the case of total binding, but instead of 20 μL of H_2O, 20 μL of a 100 μM solution of NT(8−13) in H_2O were added. It should be noted that this experimental setup corresponds to a pseudo first-order measurement as the concentration of the free ligand, being markedly higher than the receptor concentration, can be considered constant by approximation during the association reaction. Specific binding data of **21**, obtained by subtracting triplicate mean values of nonspecific binding from triplicate mean values of total binding, were plotted against the time and analyzed by a three-parameter equation describing an exponential rise to a maximum (one-phase association, Y_0 constrained to zero, GraphPad Prism 5) to yield the observed association rate constant k_{obs}. To calculate mean values in %, specific binding data were normalized based on the corresponding B_{eq} value. Since specific binding data of **19** indicated a biphasic association, data of **19** were analyzed using a five-parameter two-phase association fit (two-phase association, Y_0 constrained to zero, GraphPad Prism 5) to obtain the observed association rate constants $k_{obs(bi,fast)}$ and $k_{obs(bi,slow)}$ for the fast and slow phase of the association, respectively. To calculate mean values in % (cf. Figure 3B), specific binding data were normalized based on the corresponding B_{eq} values from the two-phase association fit (set to 100%). In addition to this analysis, the whole specific binding data of **19** were analyzed by a three-parameter equation describing an exponential rise to a maximum (one-phase association, Y_0 constrained to zero, GraphPad Prism 5) to yield the observed association rate constant $k_{obs(mono)}$.

Dissociation Experiments. 5 mL polypropylene tubes were prefilled with 2000 μL of cell suspension. For the determination of total binding, the preincubation was started by the addition of H_2O (20 μL) and a 100 nM solution of **19** or a 25 nM solution of **21** in DMSO/H_2O 2:8 v/v (20 μL) (final fluorescent ligand concentration: 1 nM (**19**) or 0.25 nM (**21**)). To determine nonspecific binding, a 100 μM solution of NT(8−13) in H_2O (20 μL) and a 100 nM solution of **19** or a 25 nM solution of **21** in DMSO/H_2O 2:8 v/v were added. The samples were gently shaken in the dark at 23 ± 1 °C for 120 min (**19**) or for 180 min (**21**). The dissociation process was initiated by the addition of a 2.5 mM solution of NT(8−13) in H_2O (20 μL) (final concentration: approximately 25 μM). After different periods of time (1−300 min (**19**) or 5−600 min (**21**)), sample aliquots were measured by placing the tube in the injection port of the flow cytometer. Specific binding data, obtained by subtracting triplicate mean values of nonspecific binding from triplicate mean values of total binding, were plotted against the time and analyzed by a three-parameter equation describing an incomplete monophasic exponential decline (one phase decay, GraphPad Prism 5) to obtain k_{off} values. For both fluorescent ligands, the mean ± SEM of the plateau values from individual experiments proved to be significantly different from zero (unpaired one-tailed *t* test, $P > 0.05$). To calculate mean values in %, binding data were normalized based on the specifically bound ligand measured immediately before the start of the dissociation.

Calculation of Association Rate Constants (k_{on}) and Kinetically Derived Dissociation Constants K_d(kin). The association rate constants were calculated from k_{obs} mean values, k_{off} mean values, and the fluorescent ligand concentration used for the association experiments ([FL]) according to the equation $k_{on} = (k_{obs} - k_{off})/[FL]$. The kinetically derived dissociation constants K_d(kin) were calculated from the respective k_{on} value and the k_{off} mean value according to $K_d(kin) = k_{off}/k_{on}$.

Competition Binding Experiments. A 96-well polypropylene plate was prefilled with 200 μL of cell suspension. 2 μL of DMSO/H_2O 2:8 v/v (for the determination of total binding in the absence of competitor), 2 μL of a 100 μM solution of NT(8−13) in H_2O (determination of nonspecific binding) or 2 μL of a 100-fold concentrated solution (compared to the final concentration) of the compound of interest (NT(8−13), SR142948, SR48692 or UR-MK300; used at varying concentrations) in DMSO/H_2O 2:8 v/v were added and the plate was shortly shaken. Subsequently, 2 μL of a 30 nM solution of **19** or a 10 nM solution of **21** in DMSO/H_2O 2:8 v/v were added to each well and the plate was gently shaken in the dark at 23 ± 1 °C for 120 min (**19**) or 180 min (**21**)

https://doi.org/10.1021/acs.jmedchem.5c01701
J. Med. Chem. XXXX, XXX, XXX−XXX

followed by measurement *via* the HTS unit. The final concentrations of **19** and **21** corresponded to their 3-fold or 2-fold K_d values determined by equilibrium saturation binding (K_d = 0.11 nM (**19**) or 0.046 nM (**21**)). Total binding fluorescence intensities (including total binding in the absence of competitor) were plotted against log (concentration inhibitor) and analyzed by a four-parameter logistic equation (log(inhibitor) vs response-variable slope, GraphPad Prism 5) to obtain pIC_{50} values. Individual pIC_{50} values were converted to pK_i values according to the Cheng-Prusoff equation[49] (logarithmic form). To plot average data from individual binding experiments, data were normalized (100% = "top" of the four-parameter logistic fit, 0% = nonspecifically bound fluorescent ligand).

Binding Experiments with SBI-553. A 96-well polypropylene plate was prefilled with 200 μL of cell suspension. 2 μL of DMSO/H_2O 2:8 v/v (determination of total binding in the absence of SBI-553) or 2 μL of a 100-fold concentrated solution (compared to the final concentration) of SBI-553 (used at varying concentrations) in DMSO/H_2O 2:8 v/v (determination of total binding in the presence of SBI-553) were added and the plate was incubated at 23 ± 1 °C for 30 min. Subsequently, 2 μL of a 1 nM solution of **21** in DMSO/H_2O 2:8 v/v (final concentration: 0.01 nM) were added. To determine nonspecific binding, 2 μL of a 100 μM solution of NT(8−13) in H_2O and 2 μL of a 1 nM solution of **21** in DMSO/H_2O 2:8 v/v were added. The plate was then gently shaken in the dark at 23 ± 1 °C for 180 min followed by measurement *via* the HTS unit. Total binding fluorescence intensities (including total binding in the absence of the allosteric modulator) were plotted against log (concentration SBI-553). As the data clearly indicated a biphasic course, data were analyzed by a five-parameter two sites—fit $logIC_{50}$ (GraphPad Prism 5) to obtain pIC_{50} (corresponding to pEC_{50}) values for the high- and low-affinity state (the biphasic fit was favored over the four-parameter logistic fit according to the *F*-test, $P < 0.05$, GraphPad Prism 5). To plot average data from individual binding experiments, data were normalized (100% = lower plateau of the initial biphasic fit, 0% = nonspecifically bound fluorescent ligand). The differences between the lower and upper plateaus of the individual experiments gave the E_{max} values which were averaged to give the E_{max} mean ± SEM.

Confocal Microscopy. Confocal microscopy was performed with a Zeiss LSM 710 confocal laser scanning microscope (Zeiss, Jena, Germany). The objective was 63× magnification with oil (1.4 NA). One day prior to the experiment, CHO-hNTS_1R (30,000 to 35,000 cells per chamber) and HT-29 cells (45,000 to 50,000 cells per chamber) were seeded in Nunc LabTekTM II cover glasses with 8 chambers (Thermo Fisher Scientific). On the day of the experiment, the confluency of the cells was 60−80%. After removal of the culture medium, cells were washed with Leibovitz's L15 medium (200 μL) and covered with L15 medium (150 μL) containing H33342 (Sigma-Aldrich) (2 μg/mL). To study total binding, L15 medium (150 μL) containing H33342 (2 μg/mL) and **19** or **21** (final concentration: 2 nM) was added. To determine nonspecific binding, L15 medium (150 μL) containing H33342 (2 μg/mL), NT(8−13) (final concentration: 1 μM) and **19** or **21** was added. The first image was acquired 5 min after addition of the fluorescent ligand. The pinhole was set to 1.0 airy unit. Laser powers and gains for the investigation of **19**: 405 nm, 2% (gain: 700 V); 561 nm, 8% (gain: 800 V) (CHO-hNTS_1R cells) or 10% (gain: 850 V) (HT-29 cells). Laser powers and gains for the study of **21**: 405 nm, 2% (gain: 650 V (HT-29 cells) or 750 V (CHO-hNTS_1R cells)); 633 nm, 20% (gain: 1050 V) (CHO-hNTS_1R cells) or 40% (gain: 1100 V) (HT-29 cells). The following filter settings for fluorescence detection were applied: 410−549 nm (H33342, experiments with **19**), 410−585 nm (H33342, experiments with **21**), 562−649 nm (**19**), and 638−759 nm (**21**).

Biomolecular Imaging. *Saturation Binding Studies at HT-29 Cells.* HT-29 cells were seeded 1 day prior to the experiment (1.0×10^5 cells/well) in black clear bottom 96-well plates (Greiner 655090, Greiner Bio-One). After washing the cells with Leibovitz's L-15 Medium (Thermo Fisher Scientific, Waltham, MA, USA), 100 μL of L-15 containing **19** or **21** in various concentrations (0.1−100 nM (**19**) or 0.1−25 nM (**21**), each in triplicates) followed by incubation at rt in the dark for 2 h. To determine nonspecific binding, SR142948 (1 μM; Sigma-Aldrich) was added to the samples. For the determination of the autofluorescence only L-15 was added to the cells. In addition, CellTag 520 or 700 Stain (LI-COR Biotechnology, Bad Homburg, Germany) was added to each well (final concentrations: 1 μM and 0.2 μM, respectively). After incubation, the plate was set on ice, the cells were washed three times with ice-cold DPBS (Sigma-Aldrich), the buffer was removed, and fluorescence images were acquired using the Sapphire FL Biomolecular Imager (520 and 658 nm laser; pixel size: 20 μm; Azure Biosystems, Dublin, CA, USA). The following bandpass filters were used for fluorescence detection: 565/24 nm (**19**) or 710/40 nm (**21**). Fluorescence intensities for each well were normalized to the respective CellTag fluorescence. Specific binding data, obtained by subtracting triplicate mean values of nonspecific binding from triplicate mean values of total binding, were plotted against the ligand concentration and K_d values were obtained by fitting of the data with a two-parameter equation describing hyperbolic single-site binding (one site, specific binding, GraphPad Prism 9). Four independent experiments were performed in triplicate.

Fluorescent Imaging of Tumor Slices. NMRI (nu/nu) mice were bred in the animal facility of the University of Regensburg. All animal experiments were performed following the protocols evaluated and approved by the local veterinary medicine authority—Regierung der Oberpfalz, Bavaria, Germany (approval number 2532.4-11/11). HT-29 tumor slices (10 μm) were prepared from HT-29 tumors (subcutaneously grown in 3−6 months old male NMRI nude (nu/nu) mice) using a cryostat microtome HM 500 O (Microm, Walldorf, Germany) and thaw-mounted on HistoBond adhesive glass slides (Marienfeld, Lauda-Königshofen, Germany). Tumor slices used for the determination of total binding were covered with buffer (DPBS supplemented with 1.8 mM $CaCl_2$ and 3.98 mM $MgCl_2$) at rt for 15 min. Tumor slices used for the determination of nonspecific binding were preincubated with buffer containing SR142948 (5 μM in buffer). The tumor slices were then incubated with **19** (10 nM) or **21** (5 nM) in buffer to determine total binding. For the determination of nonspecific binding, the samples contained additionally SR142948 (5 μM). Tumor slices were incubated with neat buffer to determine background signals (autofluorescence). After 1 h of incubation, the tumor slices were washed three times with ice-cold buffer, once with cold water, and were allowed to dry prior to acquisition of fluorescence images as described under *Saturation binding*

https://doi.org/10.1021/acs.jmedchem.5c01701
J. Med. Chem. XXXX, XXX, XXX−XXX

studies at HT-29 cells. Data analysis was performed using the Aida Image Analyzer (v.5.1, Elysia-raytest GmbH, Straubenhardt, Germany).

Calculation of Propagated Errors. Propagated errors (applying to specifically bound fluorescent ligand (saturation binding)), association rate constants k_{on}, and kinetically derived dissociation constants K_d(kin) were calculated as described elsewhere.[50]

■ ASSOCIATED CONTENT

Supporting Information

The Supporting Information is available free of charge at https://pubs.acs.org/doi/10.1021/acs.jmedchem.5c01701.

Synthesis of compounds **10**, **24**, **26**, and **27** (Scheme S1) and experimental protocols and analytical data of **10**, **24**, **26**, and **27**; structures and NTS_1R binding affinities of reported NT(8−13) derivatives containing *β*,*β*-dimethyl-L-Tyr or *β*,*β*-dimethyl-D-Tyr in position 11 (Figure S1); chemical stability of **19** and **21**: chromatograms of the HPLC analyses (Figures S2 and S3); structure of [^{3}H]UR-MK300 (Figure S4); radioligand displacement curves from competition binding experiments with [^{3}H]UR-MK300 (Figure S5); concentration response curves of NT(8−13), **19**, and **21** obtained from a Fura-2 Ca^{2+} assay (Figure S6); absorption, emission, and excitation spectra, and graphical presentation of the fluorescence decay of **19** and **21** (Figure S7); representative binding isotherms of **19** and **21** obtained from flow cytometric saturation binding experiments performed at intact CHO-hNTS_1R cells (Figure S8); visualization of binding of **19** to intact CHO-hNTS_1R cells by confocal microscopy (Figure S9); visualization of binding of **21** to intact CHO-hNTS_1R cells by confocal microscopy (Figure S10); confocal microscopy: estimation of total cellular fluorescence and intracellular fluorescence (Figure S11); fluorescence image of a 96-well plate with adherent HT-29 cells acquired with a Biomolecular Imager after incubation with **19** (Figure S12); fluorescence images of cryosections of a HT-29 tumor acquired after incubation with **19** (Figure S13); recoveries of **19** and **21** from human plasma/PBS 1:2 v/v and ratios of compound-recovery over recovery of internal standard (Table S1); electropherograms of the CE analysis of (*R*,*S*)-**10** and (*R*)-**10**; RP-HPLC chromatograms of **6**, **10**, **14**−**17b**, **19**, and **21** (purity controls); ^{1}H NMR spectrum and ^{13}C NMR spectrum of compound **10**; ^{1}H NMR spectra of compounds **14**−**17b**, **19**, and **21** and ^{13}C NMR spectra of compounds **14**−**17b** (PDF)

Molecular formula strings and NTS_1R receptor affinities (CSV)

■ AUTHOR INFORMATION

Corresponding Authors

Max Keller − *Institute of Pharmacy, Faculty of Chemistry and Pharmacy, University of Regensburg, Regensburg D-93053, Germany; Bavarian Cancer Research Center (BZKF), Translational Research Group TRAFO, Regensburg D-93053, Germany;* orcid.org/0000-0002-8095-8627; Phone: (+49) 941-9433329; Email: max.keller@chemie.uni-regensburg.de; Fax: (+49) 941-9434820

Olaf Prante − *Department of Nuclear Medicine, Molecular Imaging and Radiochemistry, Friedrich-Alexander-Universität Erlangen-Nürnberg (FAU), Erlangen D-91054, Germany; Bavarian Cancer Research Center (BZKF), Translational Research Group TRAFO, D-91054 Erlangen, Germany; FAU NeW - Research Center New Bioactive Compounds, Friedrich-Alexander-Universität Erlangen-Nürnberg (FAU), Erlangen D-91058, Germany;* orcid.org/0000-0003-0247-3656; Phone: (+49) 9131 85-44440; Email: olaf.prante@uk-erlangen.de

Roger J. Kutta − *Institute of Physical and Theoretical Chemistry, Faculty of Chemistry and Pharmacy, University of Regensburg, Regensburg D-93053, Germany*; Phone: (+49) 941-9434470; Email: roger-jan.kutta@ur.de

Authors

Fabian J. Ertl − *Institute of Pharmacy, Faculty of Chemistry and Pharmacy, University of Regensburg, Regensburg D-93053, Germany; Bavarian Cancer Research Center (BZKF), Translational Research Group TRAFO, Regensburg D-93053, Germany;* orcid.org/0000-0001-7195-4387

Anna Friedel − *Department of Nuclear Medicine, Molecular Imaging and Radiochemistry, Friedrich-Alexander-Universität Erlangen-Nürnberg (FAU), Erlangen D-91054, Germany; Bavarian Cancer Research Center (BZKF), Translational Research Group TRAFO, D-91054 Erlangen, Germany*

Elena J. Schmid − *Institute of Pharmacy, Faculty of Chemistry and Pharmacy, University of Regensburg, Regensburg D-93053, Germany*

Carina Höring − *Institute of Pharmacy, Faculty of Chemistry and Pharmacy, University of Regensburg, Regensburg D-93053, Germany;* Present Address: Roche Diagnostics GmbH, Nonnenwald 2, 82377 Penzberg, Germany

Nataliya Archipowa − *Institute of Biophysics and Physical Biochemistry, Faculty of Biology and Preclinical Medicine, University of Regensburg, Regensburg D-93053, Germany;* orcid.org/0000-0002-8519-2819

Pierre Koch − *Institute of Pharmacy, Faculty of Chemistry and Pharmacy, University of Regensburg, Regensburg D-93053, Germany;* orcid.org/0000-0003-4620-4650

Simone Maschauer − *Department of Nuclear Medicine, Molecular Imaging and Radiochemistry, Friedrich-Alexander-Universität Erlangen-Nürnberg (FAU), Erlangen D-91054, Germany; Bavarian Cancer Research Center (BZKF), Translational Research Group TRAFO, D-91054 Erlangen, Germany;* orcid.org/0000-0002-6550-933X

Complete contact information is available at: https://pubs.acs.org/10.1021/acs.jmedchem.5c01701

Author Contributions

F.J.E. and E.J.S. performed the syntheses. F.J.E. performed radiochemical binding assays, stability studies, and flow cytometric binding assays. F.J.E. and C.H. performed functional assays. N.A. and R.J.K. recorded the absorption, emission, and excitation spectra including the fluorescence decays and fluorescence quantum yields. F.J.E. and M.K. performed confocal microscopy imaging experiments. A.F. performed biomolecular imaging experiments. M.K. initiated and planned the project. M.K., O.P., P.K., S.M., and R.J.K. supervised the research. F.J.E. and M.K. wrote the manuscript with support from all co-authors. All authors have given approval to the final version of the manuscript.

https://doi.org/10.1021/acs.jmedchem.5c01701
J. Med. Chem. XXXX, XXX, XXX−XXX

Notes

The authors declare no competing financial interest.

■ ACKNOWLEDGMENTS

The authors thank Maria Beer-Krön, Susanne Bollwein, Annalena Wein, Brigitte Wenzl, and Manuel Geisthoff for excellent technical support, and Peter Gmeiner and Harald Hübner (Department of Chemistry and Pharmacy, FAU Erlangen) for providing CHO-hNTS$_1$R cells. This project was supported by the Deutsche Forschungsgemeinschaft (DFG) (research grant KE 1857/1-3) and by the Bavarian Cancer Research Center (BZKF) (translational research group TRAFO, TG-014).

■ ABBREVIATIONS

AF, autofluorescence; Arg(carb), N^{ω}-carbamoylated arginine; CE, capillary electrophoresis; CEC, concentration-effect curve; CH_2Cl_2, dichloromethane; CHO cells, Chinese hamster ovary cells; 2-ClTrt, 2-chlorotrityl; DPBS, Dulbecco's phosphate buffered saline; DIPEA, diisopropylethylamine; FBS, fetal bovine serum; FC, flow cytometry; HBTU, [bis-(dimethylamino)methyliumyl]-3*H*-benzotriazol-1-oxide hexafluorophosphate; HOBt, hydroxybenzotriazole; K_d, dissociation constant from a saturation binding experiment; k_{obs}, observed association rate constant; k_{off}, dissociation rate constant; k_{on}, association rate constant; MTBD, methyl-1,5,7-triazabicyclo[4.4.0]dec-5-ene; NEAA, non essential amino acid solution; NTS$_1$R, neurotensin receptor type 1; pEC_{50}, negative decadic logarithm of the half maximal effective concentration (functional assays); pK_i, negative decadic logarithm of the dissociation constant K_i (in nM) obtained from a competition binding experiment; ROI, region of interest; SEM, standard error of the mean; SPPS, solid phase peptide synthesis; TMSAla, (trimethylsilyl)alanine

■ REFERENCES

(1) Carraway, R.; Leeman, S. E. The isolation of a new hypotensive peptide, neurotensin, from bovine hypothalami. *J. Biol. Chem.* **1973**, *248*, 6854−6861.
(2) Vita, N.; Laurent, P.; Lefort, S.; Chalon, P.; Dumont, X.; Kaghad, M.; Gully, D.; Le Fur, G.; Ferrara, P.; Caput, D. Cloning and expression of a complementary DNA encoding a high affinity human neurotensin receptor. *FEBS Lett.* **1993**, *317*, 139−142.
(3) Vincent, J. P.; Mazella, J.; Kitabgi, P. Neurotensin and neurotensin receptors. *Trends Pharmacol. Sci.* **1999**, *20*, 302−309.
(4) Reubi, J. C.; Waser, B.; Friess, H.; Buchler, M.; Laissue, J. Neurotensin receptors: A new marker for human ductal pancreatic adenocarcinoma. *Gut* **1998**, *42*, 546−550.
(5) Yin, X.; Wang, M.; Wang, H.; Deng, H.; He, T.; Tan, Y.; Zhu, Z.; Wu, Z.; Hu, S.; Li, Z. Evaluation of neurotensin receptor 1 as a potential imaging target in pancreatic ductal adenocarcinoma. *Amino Acids* **2017**, *49*, 1325−1335.
(6) He, T.; Wang, M.; Wang, H.; Tan, H.; Tang, Y.; Smith, E.; Wu, Z.; Liao, W.; Hu, S.; Li, Z. Evaluation of neurotensin receptor 1 as potential biomarker for prostate cancer theranostic use. *Eur. J. Nucl. Med. Mol. Imaging* **2019**, *46*, 2199−2207.
(7) Morgat, C.; Brouste, V.; Chastel, A.; Velasco, V.; Macgrogan, G.; Hindie, E. Expression of neurotensin receptor-1 (NTS$_1$) in primary breast tumors, cellular distribution, and association with clinical and biological factors. *Breast Cancer Res. Treat.* **2021**, *190*, 403−413.
(8) Szarynska, M.; Olejniczak-Keder, A.; Podplonska, K.; Prahl, A.; Ilowska, E. Bradykinin and neurotensin analogues as potential compounds in colon cancer therapy. *Int. J. Mol. Sci.* **2023**, *24* (11), 9644.
(9) Pan, M.; Chen, Q.; Yao, S. Recent advances in small molecular PET tracers for pancreatic cancer diagnosis: preclinical stage. *Mini-Rev. Med. Chem.* **2025**, *25*, 745−759.
(10) Maschauer, S.; Prante, O. Radiopharmaceuticals for imaging and endoradiotherapy of neurotensin receptor-positive tumors. *J. Labelled Compd. Radiopharm.* **2018**, *61*, 309−325.
(11) Maes, V.; Hultsch, C.; Kohl, S.; Bergmann, R.; Hanke, T.; Tourwé, D. Fluorescein-labeled stable neurotensin derivatives. *J. Pept. Sci.* **2006**, *12*, 505−508.
(12) Keller, M.; Kuhn, K. K.; Einsiedel, J.; Hübner, H.; Biselli, S.; Mollereau, C.; Wifling, D.; Svobodová, J.; Bernhardt, G.; Cabrele, C.; et al. Mimicking of arginine by functionalized N^{ω}-carbamoylated arginine as a new broadly applicable approach to labeled bioactive peptides: High affinity angiotensin, neuropeptide Y, neuropeptide FF, and neurotensin receptor ligands as examples. *J. Med. Chem.* **2016**, *59* (5), 1925−1945.
(13) Keller, M.; Mahuroof, S. A.; Hong Yee, V.; Carpenter, J.; Schindler, L.; Littmann, T.; Pegoli, A.; Hübner, H.; Bernhardt, G.; Gmeiner, P.; Holliday, N. D. Fluorescence labeling of neurotensin(8−13) via arginine residues gives molecular tools with high receptor affinity. *ACS Med. Chem. Lett.* **2020**, *11*, 16−22.
(14) Renard, E.; Dancer, P. A.; Portal, C.; Denat, F.; Prignon, A.; Goncalves, V. Design of bimodal ligands of neurotensin receptor 1 for positron emission tomography imaging and fluorescence-guided surgery of pancreatic cancer. *J. Med. Chem.* **2020**, *63*, 2426−2433.
(15) Grätz, L.; Müller, C.; Pegoli, A.; Schindler, L.; Bernhardt, G.; Littmann, T. Insertion of nanoluc into the extracellular loops as a complementary method to establish BRET-based binding assays for GPCRs. *ACS Pharmacol. Transl. Sci.* **2022**, *5*, 1142−1155.
(16) Ertlü, F. J.; Kopanchuk, S.; Dijon, N. C.; Veiksina, S.; Tahk, M. J.; Laasfeld, T.; Schettler, F.; Gattor, A. O.; Hübner, H.; Archipowa, N.; Köckenberger, J.; Heinrich, M. R.; Gmeiner, P.; Kutta, R. J.; Holliday, N. D.; Rinken, A.; Keller, M. Dually labeled neurotensin NTS$_1$R ligands for probing radiochemical and fluorescence-based binding assays. *J. Med. Chem.* **2024**, *67*, 16664−16691.
(17) Skrzydelski, D.; Lhiaubet, A. M.; Lebeau, A.; Forgez, P.; Yamada, M.; Hermans, E.; Rostene, W.; Pelaprat, D. Differential involvement of intracellular domains of the rat NTS1 neurotensin receptor in coupling to G proteins: a molecular basis for agonist-directed trafficking of receptor stimulus. *Mol. Pharmacol.* **2003**, *64*, 421−429.
(18) Granier, C.; van Rietschoten, J.; Kitabgi, P.; Poustis, C.; Freychet, P. Synthesis and characterization of neurotensin analogues for structure/activity relationship studies. Acetyl-neurotensin-(8−13) is the shortest analogue with full binding and pharmacological activities. *Eur. J. Biochem.* **1982**, *124*, 117−124.
(19) Fanelli, R.; Besserer-Offroy, E.; Rene, A.; Cote, J.; Tetreault, P.; Collerette-Tremblay, J.; Longpre, J. M.; Leduc, R.; Martinez, J.; Sarret, P.; Cavelier, F. Synthesis and characterization in vitro and in vivo of (L)-(trimethylsilyl)alanine containing neurotensin analogues. *J. Med. Chem.* **2015**, *58*, 7785−7795.
(20) Vivancos, M.; Fanelli, R.; Besserer-Offroy, E.; Beaulieu, S.; Chartier, M.; Resua-Rojas, M.; Mona, C. E.; Previti, S.; Remond, E.; Longpre, J. M.; Cavelier, F.; Sarret, P. Metabolically stable neurotensin analogs exert potent and long-acting analgesia without hypothermia. *Behav. Brain Res.* **2021**, *405*, 113189.
(21) Schindler, L.; Moosbauer, J.; Schmidt, D.; Spruss, T.; Grätz, L.; Lüdeke, S.; Hofheinz, F.; Meister, S.; Echtenacher, B.; Bernhardt, G.; Pietzsch, J.; Hellwig, D.; Keller, M. Development of a neurotensin-derived ^{68}Ga-labeled PET ligand with high in vivo stability for imaging of NTS$_1$ receptor-expressing tumors. *Cancers* **2022**, *14*, 4922.
(22) Schindler, L.; Bernhardt, G.; Keller, M. Modifications at Arg and Ile give neurotensin(8−13) derivatives with high stability and retained NTS$_1$ receptor affinity. *ACS Med. Chem. Lett.* **2019**, *10*, 960−965.
(23) Rene, A.; Vanthuyne, N.; Martinez, J.; Cavelier, F. (L)-(Trimethylsilyl)alanine synthesis exploiting hydroxypinanone-induced diastereoselective alkylation. *Amino Acids* **2013**, *45*, 301−307.

https://doi.org/10.1021/acs.jmedchem.5c01701
J. Med. Chem. XXXX, XXX, XXX−XXX

(24) Miller, S. C.; Scanlan, T. S. Site-selective N-methylation of peptides on solid support. *J. Am. Chem. Soc.* **1997**, *119*, 2301−2302.
(25) Archipowa, N.; Wittmann, L.; Köckenberger, J.; Ertl, F. J.; Gleixner, J.; Keller, M.; Heinrich, M. R.; Kutta, R. J. Characterization of fluorescent dyes frequently used for bioimaging: Photophysics and photocatalytical reactions with proteins. *J. Phys. Chem. B* **2023**, *127*, 9532−9542.
(26) Lugrin, D.; Vecchini, F.; Doulut, S.; Rodriguez, M.; Martinez, J.; Kitabgi, P. Reduced peptide bond pseudopeptide analogues of neurotensin: Binding and biological activities, and in vitro metabolic stability. *Eur. J. Pharmacol.* **1991**, *205*, 191−198.
(27) Cusack, B.; McCormick, D. J.; Pang, Y. P.; Souder, T.; Garcia, R.; Fauq, A.; Richelson, E. Pharmacological and biochemical profiles of unique neurotensin 8−13 analogs exhibiting species selectivity, stereoselectivity, and superagonism. *J. Biol. Chem.* **1995**, *270*, 18359−18366.
(28) Einsiedel, J.; Held, C.; Hervet, M.; Plomer, M.; Tschammer, N.; Hübner, H.; Gmeiner, P. Discovery of highly potent and neurotensin receptor 2 selective neurotensin mimetics. *J. Med. Chem.* **2011**, *54*, 2915−2923.
(29) Previti, S.; Vivancos, M.; Remond, E.; Beaulieu, S.; Longpre, J.-M.; Ballet, S.; Sarret, P.; Cavelier, F. Insightful backbone modifications preventing proteolytic degradation of neurotensin analogs improve NTS1-induced protective hypothermia. *Front. Chem.* **2020**, *8*, 406.
(30) Grynkiewicz, G.; Poenie, M.; Tsien, R. Y. A new generation of Ca2+ indicators with greatly improved fluorescence properties. *J. Biol. Chem.* **1985**, *260*, 3440−3450.
(31) Müller, C.; Gleixner, J.; Tahk, M. J.; Kopanchuk, S.; Laasfeld, T.; Weinhart, M.; Schollmeyer, D.; Betschart, M. U.; Lüdeke, S.; Koch, P.; Rinken, A.; Keller, M. Structure-based design of high-affinity fluorescent probes for the neuropeptide Y Y(1) receptor. *J. Med. Chem.* **2022**, *65*, 4832−4853.
(32) Köckenberger, J.; Fischer, O.; Konopa, A.; Bergwinkl, S.; Mühlich, S.; Gmeiner, P.; Kutta, R. J.; Hübner, H.; Keller, M.; Heinrich, M. R. Synthesis, characterization, and application of muscarinergic M_3 receptor ligands linked to fluorescent dyes. *J. Med. Chem.* **2022**, *65*, 16494−16509.
(33) She, X. K.; Pegoli, A.; Gruber, C. G.; Wifling, D.; Carpenter, J.; Hübner, H.; Chen, M. Y.; Wan, J. F.; Bernhardt, G.; Gmeiner, P.; Holliday, N. D.; Keller, M. Red-emitting dibenzodiazepinone derivatives as fluorescent dualsteric probes for the muscarinic acetylcholine M_2 receptor. *J. Med. Chem.* **2020**, *63*, 4133−4154.
(34) Carter, C. M. S.; Ies, C. R. L. D.; Charlton, S. J. Miniaturized receptor binding assays: Complications arising from ligand depletion. *SLAS Discovery* **2007**, *12*, 255−266.
(35) Maschauer, S.; Einsiedel, J.; Hübner, H.; Gmeiner, P.; Prante, O. ^{18}F- and ^{68}Ga-Labeled neurotensin peptides for PET imaging of neurotensin receptor 1. *J. Med. Chem.* **2016**, *59*, 6480−6492.
(36) Lang, C.; Maschauer, S.; Hübner, H.; Gmeiner, P.; Prante, O. Synthesis and evaluation of a ^{18}F-labeled diarylpyrazole glycoconjugate for the imaging of NTS1-positive tumors. *J. Med. Chem.* **2013**, *56*, 9361−9365.
(37) Pugsley, T. A.; Akunne, H. C.; Whetzel, S. Z.; Demattos, S.; Corbin, A. E.; Wiley, J. N.; Wustrow, D. J.; Wise, L. D.; Heffner, T. G. Differential effects of the nonpeptide neurotensin antagonist, SR 48692, on the pharmacological effects of neurotensin agonists. *Peptides* **1995**, *16*, 37−44.
(38) Prinz, H. Hill coefficients, dose-response curves and allosteric mechanisms. *J. Biol. Chem.* **2010**, *3*, 37−44.
(39) Bindslev, N. *Drug-acceptor interactions: modeling theoretical tools to test and evaluate experimental equilibirum effects, open access e-book*; Taylor & Francis Group, 2017.
(40) Deluigi, M.; Klipp, A.; Klenk, C.; Merklinger, L.; Eberle, S. A.; Morstein, L.; Heine, P.; Mittl, P. R. E.; Ernst, P.; Kamenecka, T. M.; et al. Complexes of the neurotensin receptor 1 with small-molecule ligands reveal structural determinants of full, partial, and inverse agonism. *Sci. Adv.* **2021**, *7*, No. eabe5504.
(41) Lu, X.; Shi, X.; Fan, J.; Li, M.; Zhang, Y.; Lu, S.; Xu, G.; Chen, Z. Mechanistic elucidation of activation/deactivation signal transduction within neurotensin receptor 1 triggered by 'Driver Chemical Groups' of modulators: A comparative molecular dynamics simulation. *Pharmaceutics* **2023**, *15*, 2000.
(42) Pinkerton, A. B.; Peddibhotla, S.; Yamamoto, F.; Slosky, L. M.; Bai, Y.; Maloney, P.; Hershberger, P.; Hedrick, M. P.; Falter, B.; Ardecky, R. J.; Smith, L. H.; Chung, T. D. Y.; Jackson, M. R.; Caron, M. G.; Barak, L. S. Discovery of beta-arrestin biased, orally bioavailable, and CNS penetrant neurotensin receptor 1 (NTR1) allosteric modulators. *J. Med. Chem.* **2019**, *62*, 8357−8363.
(43) Slosky, L. M.; Bai, Y.; Toth, K.; Ray, C.; Rochelle, L. K.; Badea, A.; Chandrasekhar, R.; Pogorelov, V. M.; Abraham, D. M.; Atluri, N.; et al. beta-Arrestin-biased allosteric modulator of NTSR1 selectively attenuates addictive behaviors. *Cell* **2020**, *181* (6), 1364−1379e1314.
(44) Vogt, H.; Shinkwin, P.; Huber, M. E.; Staffen, N.; Hübner, H.; Gmeiner, P.; Schiedel, M.; Weikert, D. Development of a fluorescent ligand for the intracellular allosteric binding site of the neurotensin receptor 1. *ACS Pharmacol. Transl. Sci.* **2024**, *7*, 1533−1545.
(45) Guo, R.; Chen, O.; Zhou, Y.; Bang, S.; Chandra, S.; Li, Y.; Chen, G.; Xie, R.-G.; He, W.; Xu, J.; et al. Arrestin-biased allosteric modulator of neurotensin receptor 1 alleviates acute and chronic pain. *Cell* **2025**, *188* (16), 4332−4349.e21.
(46) Fanelli, R.; Chastel, A.; Previti, S.; Hindie, E.; Vimont, D.; Zanotti-Fregonara, P.; Fernandez, P.; Garrigue, P.; Lamare, F.; Schollhammer, R.; Balasse, L.; Guillet, B.; Remond, E.; Morgat, C.; Cavelier, F. Silicon-containing neurotensin analogues as radiopharmaceuticals for NTS_1-positive tumors imaging. *Bioconjugate Chem.* **2020**, *31*, 2339−2349.
(47) Gude, M.; Ryf, J.; White, P. D. An accurate method for the quantitation of Fmoc-derivatized solid phase supports. *Lett. Pept. Sci.* **2002**, *9*, 203−206.
(48) Kutta, R. J. *Blitzlichtphotolyse - Untersuchung zu LOV-Domänen und photochromen Systemen* Doctoral Thesis; University of Regensburg: Regensburg, Germany, 2012. https://epub.uni-regensburg.de/24528/1/Dissertation_main_online.pdf.
(49) Cheng, Y.-C.; Prusoff, W. H. Relationship between the inhibition constant (K_I) and the concentration of inhibitor which causes 50% inhibition (IC_{50}) of an enzymatic reaction. *Biochem. Pharmacol.* **1973**, *22*, 3099−3108.
(50) Gleixner, J.; Gattor, A. O.; Humphrys, L. J.; Brunner, T.; Keller, M. [^{3}H]UR-JG102-A radiolabeled cyclic peptide with high affinity and excellent selectivity for the neuropeptide Y Y_4 receptor. *J. Med. Chem.* **2023**, *66*, 13788−13808.

https://doi.org/10.1021/acs.jmedchem.5c01701
J. Med. Chem. XXXX, XXX, XXX−XXX